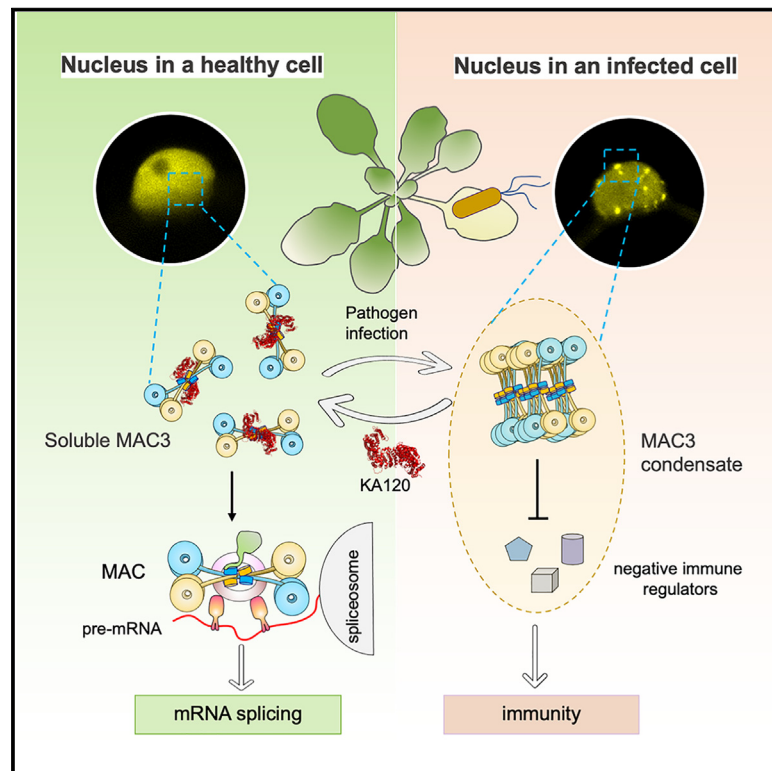


Cell Host & Microbe

Nuclear transport receptor KA120 regulates molecular condensation of MAC3 to coordinate plant immune activation

Graphical abstract



Authors

Min Jia, Xuanyi Chen, Xuetao Shi, Yiling Fang, Yangnan Gu

Correspondence

guyangnan@berkeley.edu

In brief

Jia et al. report that KA120, a conserved nuclear transport receptor, processes a noncanonical chaperoning activity to prevent spontaneous nuclear condensation of the MAC protein complex, an essential regulator of pre-mRNA splicing. However, pathogen infection triggers MAC condensate assembly in plants, sequestering negative immune regulators to coordinate host defense response.

Highlights

- Loss of KA120 leads to MAC-dependent autoimmune activation in plants
- KA120 interacts with MAC proteins and prevents spontaneous nuclear condensation of MAC
- MAC condensation is robustly induced by pathogen-triggered immune activation
- The assembly of MAC condensates is sufficient to activate defense response in plants

Article

Nuclear transport receptor KA120 regulates molecular condensation of MAC3 to coordinate plant immune activation

Min Jia,^{1,2} Xuanyi Chen,³ Xuetao Shi,⁴ Yiling Fang,^{1,2} and Yangnan Gu^{1,2,5,*}

¹Department of Plant and Microbial Biology, University of California, Berkeley, Berkeley, CA 94720, USA

²Innovative Genomics Institute, University of California, Berkeley, Berkeley, CA 94720, USA

³National Key Laboratory of Crop Improvement for Stress Tolerance and Production, College of Life Sciences, Northwest A&F University, Yangling, Shaanxi 712100, China

⁴Tsinghua-Peking Joint Center for Life Sciences, Center for Plant Biology, School of Life Sciences, Tsinghua University, Beijing 100084, China

⁵Lead contact

*Correspondence: guyangnan@berkeley.edu

<https://doi.org/10.1016/j.chom.2023.08.015>

SUMMARY

The nucleocytoplasmic exchange is of fundamental importance to eukaryotic life and is mediated by karyopherins, a superfamily of nuclear transport receptors. However, the function and cargo spectrum of plant karyopherins are largely obscure. Here, we report proximity-labeling-based proteomic profiling of *in vivo* substrates of KA120, a karyopherin- β required for suppressing autoimmune induction in *Arabidopsis*. We identify multiple components of the MOS4-associated complex (MAC), a conserved splicing regulatory protein complex. Surprisingly, we find that KA120 does not affect the nucleocytoplasmic distribution of MAC proteins but rather prevents their protein condensation in the nucleus. Furthermore, we demonstrate that MAC condensation is robustly induced by pathogen infection, which is sufficient to activate defense gene expression, possibly by sequestering negative immune regulators via phase transition. Our study reveals a noncanonical chaperoning activity of a plant karyopherin, which modulates the nuclear condensation of an evolutionarily conserved splicing regulatory complex to coordinate plant immune activation.

INTRODUCTION

Plants evolved a highly effective innate immune system to defend against assorted pathogens. Cell-surface-localized receptor-like kinases and receptor-like proteins, collectively named pattern recognition receptors (PRRs), sense conserved pathogen/microbe-derived molecular patterns and activate pattern-triggered immunity (PTI). Although pathogens have evolved a plethora of secreted proteins termed effectors to undermine host PTI, plants express a second group of immune receptors named nucleotide-binding leucine-rich repeat (NLR) proteins. NLRs directly or indirectly recognize pathogen effectors and activate effector-triggered immunity (ETI) to restrict pathogen growth.^{1–3} Emerging evidence supports that PTI and ETI are intimately connected, share comprehensive downstream components, and synergistically enhance each other.^{4,5} The integrated plant immune network has been shown to be extremely complicated and engage a diverse array of other cellular and biochemical processes, including but not limited to membrane trafficking, hormone signaling, circadian rhythm, biomolecular condensation, etc., to coordinate immune induction and optimize the defense output.^{6–11}

Previous genetic analyses show that the MOS4-associated complex (MAC), an evolutionarily conserved multifunctional protein complex, plays an essential role in plant immune activa-

tion.^{12,13} The MAC is known as the nineteen complex or PRE-mRNA PROCESSING FACTOR 19 (Prp19) complex in humans and yeasts, named after its core protein component Prp19, a U-box E3 ligase. The Prp19 complex associates with the spliceosome and mediates non-proteolytic ubiquitination of small nuclear ribonucleoprotein particle (snRNP) components to facilitate conformational changes and rearrangement of spliceosome required for the splicing reactions.^{14,15} The Prp19 complex has also emerged as a crucial component involved in DNA damage responses, including DNA damage sensation and subsequent DNA repair.^{16,17} All core components of the *Arabidopsis* MAC, including MOS4, MAC3A/B (homologs of Prp19), MAC1/CDC5, and MAC2/PRL1, have been reported to be required for both basal resistance and immune activation mediated by some NLRs, including SUPPRESSOR OF npr1-1, Constitutive 1 (SNC1), and they likely function upstream or separately from the salicylic acid (SA)-dependent immunity amplification.^{12,13} In addition, the loss of MAC5A, an accessory MAC component, can also suppress autoimmune phenotypes caused by autoactive NLR *snc1-1*.¹⁸ CDC5, PRL1, MOS4, and MAC3 were shown required for the proper splicing of NLR gene *SNC1* and *RPS4*¹⁹; however, the detailed molecular mechanism of how the MAC participates in immune regulation in plant cells is not completely understood.

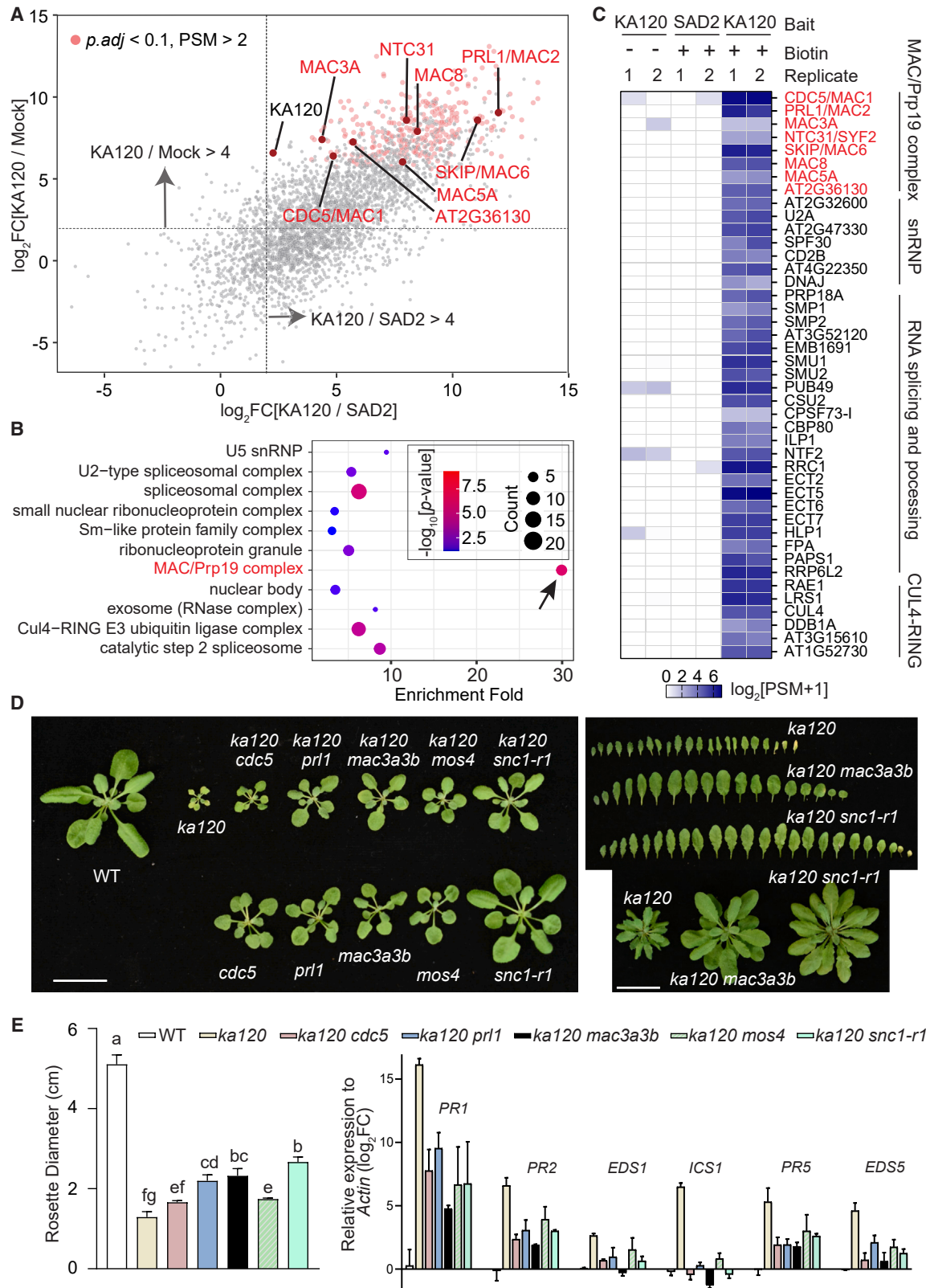


Figure 1. KA120 physically and genetically interacts with the MAC

(A) Scatter plot showing significantly enriched proteins identified by proximity-labeling proteomics using *pKA120-KA120-TurboID* transgenic *Arabidopsis* plants. Mock-treated *KA120-TurboID* plants and biotin-treated *SAD2-TurboID* transgenic plants were used as controls for ratiometric analysis. Two biological replicates

(legend continued on next page)

Although plants possess robust defensive tools, they have also evolved intricate mechanisms to prevent autoimmune activation, which is crucial to avoid misfiring and growth compromise in the absence of pathogens. These mechanisms have been revealed by extensive investigation of autoimmune mutants.^{20,21} Among them, karyopherin- β family proteins appear to play an essential role. Karyopherin- β s are nuclear transport receptors that mediate the passage of macromolecules across the nuclear pore. In *Arabidopsis*, at least three importin- β s have been shown necessary for preventing autoimmune activation.²² Exportin-4 (XPO4) was reported to negatively regulate SA-dependent immune amplification via coordinating nuclear export of transcription repressors TOPLESS and TOPLESS-related proteins.²³ Loss of KA120 and IMB2 both result in severe autoimmune phenotypes and strong defense gene expression in *Arabidopsis*.^{24,25} Previously, we demonstrated that KA120 suppresses the nuclear activity of the NLR immune receptor SNC1; however, it is unclear whether SNC1 is a direct cargo of KA120. Therefore, how KA120 and IMB2 regulate immune suppression and whether the process depends on karyopherins' cargo transport activity remain prominent questions.

In this study, we profiled *in vivo* cargo of KA120 using proximity-labeling proteomics and identified the MAC as the most enriched protein complex. Genetic analysis showed that mutations in core MAC components can substantially suppress *ka120*-dependent autoimmune phenotypes, suggesting MAC proteins as *bona fide* substrates of KA120. However, instead of affecting the nucleocytoplasmic distribution of MAC proteins, we found that KA120 is required for suppressing the nuclear condensation of the core MAC component MAC3. KA120 does so by interacting with the U-box domain of MAC3, potentially inhibiting the exposure of the adjacent coiled-coil (CC) domain that is necessary and sufficient to drive the MAC3 condensation. Remarkably, we found that although the condensate assembly compromises MAC's canonical function in mRNA splicing and DNA repair, its formation is tightly correlated with immune activation, possibly through recruiting and sequestering multiple negative immune regulators, including IMMUNOREGULATORY RNA-BINDING PROTEIN (IRR) and JASMONIC ACID OXIDASE 2 (JAO2). Finally, we showed that MAC3 condensates are robustly induced by pathogen-triggered immune activation and can be inhibited by KA120 overexpression, and the inhibition leads to enhanced disease susceptibility. Together, our results revealed a type of previously uncharacterized immune-activating nuclear condensate, whose dynamics is regulated by unconventional chaperoning activity of a plant karyopherin.

RESULTS

Identification of the MAC in the KA120 proximiome

To understand how KA120 participates in plant immune regulation, we sought to determine *in vivo* substrates of KA120. We leveraged an enzyme-catalyzed proximity-labeling strategy, in which we fused KA120 with TurboID,²⁶ an engineered promiscuous biotin ligase (Figure S1A). We generated stable transgenic *Arabidopsis* plants expressing native promoter-driven *KA120-TurboID-HA* and used T3 homozygous plants that fully complemented the *ka120* mutant phenotype to perform the proximity-labeling proteomics (Figures S1B and S1C). To identify KA120-specific substrates, we also generated transgenic plants expressing TurboID-tagged SENSITIVE TO ABA AND DROUGHT 2 (SAD2), a karyopherin homolog of KA120, and run the SAD2-TurboID sample in parallel as control. We expected KA120 and SAD2 to have largely different substrate populations because their loss-of-function mutants display distinct phenotypes.²⁴ In addition, KA120 is mainly localized to the nucleus with minor cytosolic distribution, whereas SAD2 exhibits an opposite nucleocytoplasmic distribution pattern in transgenic *Arabidopsis* (Figure S1D).

After obtaining the label-free quantitative mass spectrometry (LFQMS) data, we selected proteins that are significantly enriched in biotin-treated KA120-TurboID samples by comparing the peptide spectrum match (PSM) level with water-treated KA120-TurboID (mock) samples and biotin-treated SAD2-TurboID samples using cutoff fold-change (FC) > 4, p value < 0.1, and PSM > 2 (Figure 1A). A total of 289 protein candidates were identified (Table S1, ProteomeXchange: PXD040403). Among them, we found two importin- α s (IMAs), which are known to interact with importin- β s.^{27,28} Notably, gene ontology (GO) analysis of the 289 candidates revealed that pre-mRNA splicing and processing-related protein and protein complexes are highly enriched in the KA120 proximiome (Figure 1B). In particular, the MAC is the top-ranked protein complex with the highest and most significant enrichment, and almost half of all reported *Arabidopsis* MAC components were probed, including MAC1/CDC5 (CELL DIVISION CYCLE 5), MAC2/PRL1 (PLEIOTROPIC REGULATORY LOCUS 1), MAC3A, MAC5A, MAC6/SKIP (SKI INTERACTING PROTEIN), MAC8, NTC31/SYF2, and another MAC-associated component (AT2G36130)²⁹ (Figure 1C). This result is supported by an independently performed proximity-labeling proteomics using KA120-BioID2 (albeit less efficient than TurboID), where KA120 specifically probed another MAC core component, MAC3B (Figure S1E).

The MAC is known as the Prp19 complex in animals, which is an evolutionarily conserved nuclear protein complex and plays a critical role in the catalytic activation of spliceosomes and

were used for each sample. KA120-specific preys were selected using p value < 0.1 (linear model F tests, n = 2), fold change (FC) > 4 (for both controls), and peptide spectrum match (PSM) > 2 as cutoffs and are represented as red and pink dots. Identified MAC proteins are labeled in red.

(B) Gene ontology (GO) analysis of KA120 proximiome. Representative GO terms are shown.

(C) Heatmap showing normalized PSM values of mRNA splicing and processing-related proteins identified in the KA120 proximiome. Components of the MAC/Prp19 complex are labeled in red.

(D) 4-week-old (left panel) and 7-week-old (right panel) soil-grown WT, *ka120-1*, *snc1-r1*, *mac* mutants, and *ka120 mac* double or triple mutant plants. Scale bars, 2 cm.

(E) Measurement of rosette diameter (left panel) and the relative expression of defense marker genes using RT-qPCR (right panel) in 4-week-old plants. Data are presented as mean \pm SD (n = 3). Statistical analysis was performed using one-way ANOVA followed by Tukey's multiple comparison tests. Similar results were obtained twice.

See also Figure S1 and Table S1.

DNA repair.³⁰ Consistent with the close association between KA120 and the MAC, six snRNP and snRNP-related proteins, and more than 22 other nuclear proteins that are directly involved in RNA splicing and processing were also enriched in the KA120 proximiome (Figure 1C). In addition, we identified components of the Cullin 4 (CUL4) E3 ligases, including DAMAGED DNA BINDING PROTEIN 1A (DDB1A), a protein that directly associates with the MAC.³¹ Together, these proteomic analyses support a direct association of KA120 with the MAC *in vivo* and indicate that KA120 may functionally connect with the MAC.

The MAC is required for the *ka120*-mediated autoimmune induction

To determine the functional connection between KA120 and the MAC, we obtained transfer DNA (T-DNA) insertion mutants for multiple MACs, including the *cdc5-1*, *prl1-2*, and *mos4-1* single mutant and the *mac3a mac3b* double mutant^{12,13} and crossed them with the *ka120* mutant. We also generated a *mac8* CRISPR mutant in the *ka120* background. We found that mutations in core MAC genes, including *MAC3*, *CDC5*, *PRL1*, and *MOS4*, were able to at least partially suppress the autoimmune phenotype exhibited by the *ka120* mutant (Figures 1D and S1F). In particular, mutations in the MAC scaffolding genes (*mac3a mac3b* double mutant) significantly suppress the stunted growth and serrated and wrinkled leaves of the *ka120* mutant. Moreover, defense gene expression was substantially reduced in the *ka120 mac3a mac3b* triple mutant compared with the *ka120* single mutant (Figure 1E).

MAC components are required for the full activity of an autoactive form of the NLR protein SNC1.^{12,13} Interestingly, we previously showed that the loss-of-function *snc1-r1* mutant also suppresses the *ka120* autoimmune phenotype²⁴ to a similar extent to the *mac3a mac3b* double mutant (Figures 1D and 1E). To determine whether SNC1 and the MAC work in the same pathway or contribute independently to the *ka120*-dependent autoimmunity, we generated *ka120 mac3a mac3b snc1-r1* quadruple mutant. The quadruple mutant displayed a similar phenotype as the *ka120 mac3a mac3b* triple mutant and did not further suppress the stunted growth or defense gene expression in *ka120* plants in a significant manner (Figures S1G and S1H). This result suggests that the MAC and SNC1 may function in the same pathway to activate *ka120*-dependent autoimmunity. Considering the physical proximity between KA120 and the MAC, the above results prompt us to propose that the MAC is a direct substrate of KA120 and KA120 may negatively regulate MAC function to suppress immune activation in plants.

MAC3 forms a type of previously uncharacterized nuclear condensates in the absence of KA120

Next, we investigated how KA120 may negatively regulate MAC activity. Because KA120 encodes a karyopherin, we first tested whether KA120 affects the nucleocytoplasmic distribution of MAC proteins. To this end, we generated a translational fusion of CDC5, PRL1, MAC3B, MOS4, SKIP, and MAC8 to green fluorescent protein (GFP). These constructs were driven by their own promoters and transformed into the *ka120* heterozygous background. We selected T1 transformants that are *ka120* heterozygous and obtained T2 isogenic MAC-GFP lines in both wild-type (WT) and *ka120* backgrounds through segregation. We

found that all tested MAC-GFP proteins were predominantly distributed in the nucleus in both WT and *ka120* backgrounds (Figure 2A). Moreover, we introduced these MAC-GFP transgenes into a *KA120-mCherry* overexpression line and found that the nuclear localization of MAC proteins was not affected either (Figure S2A). These data suggest that KA120 does not affect the homeostatic nucleocytoplasmic distribution of MAC proteins.

Interestingly, although the nuclear localization of MAC proteins was not affected, we found the MAC core scaffold component MAC3B forms observable nuclear condensates in majority of cells observed in the *ka120* background. In contrast, MAC3B exhibits a uniform nuclear distribution in almost all WT nuclei (Figure 2A). A similar phenomenon was recorded using protoplast transient expression assays, with MAC3B-GFP condensates formed in over 80% of transformed *ka120* protoplasts but rarely in WT (Figures 2B and 2C). We named these condensates MAC3-dependent nuclear condensates (MDNCs). Formation of MDNCs depends specifically on the loss of KA120 but not other karyopherin- β s including SAD2 or IMB5 (Figure 2C), consistent with the finding that MAC3B is a specific substrate of KA120.

To confirm that the MDNC formation is directly correlated with the KA120 level, we transformed a dexamethasone-inducible artificial microRNA construct targeting KA120 into a 35S:MAC3B-GFP line. We treated 5-day-old transgenic seedlings with 25 μ M dex or water (mock) for 12 h before fluorescence imaging. Indeed, we observed that dex treatment induced robust formation of MDNCs (Figure 2D), whereas the protein level of MAC3B was not significantly affected (Figure S2B), suggesting that MAC3B undergoes condensation when the KA120 level is downregulated. Fluorescence quantification indicates that those condensates account for nearly 40% of MAC3B-GFP signal in the nucleus (Figure S2C), suggesting a major transformation of MAC3B from a soluble state to condensates.

Using time-lapse microscopy, we found that MDNCs undergo dynamic fusion events (Figure 2E). fluorescence recovery after photobleaching (FRAP) analysis further revealed that most photobleached MDNCs were able to recover within 2 min (Figure 2F), suggesting active exchange of materials of the MDNC with its environment. These properties are highly consistent with biomolecular condensates whose formation is driven by liquid-liquid phase separation (LLPS).

To explore the identity of the MDNC as a nuclear condensate, we transformed the 35S:MAC3B-GFP/Dex:amiRNA-KA120 double transgenic line with three known markers that label different nuclear condensates, including HYL1-mCherry for dicing bodies,³² SR45-mRFP for splicing bodies,³³ and Collin-mCherry for Cajal bodies.³⁴ We then induced MDNC formation using dex to observe potential co-localization. However, we found no significant overlap between MDNCs with any of the tested markers (Figure S2D), suggesting that MDNCs may form a distinct population of nuclear condensates that is different from well-defined nuclear condensates in plants. Because the MDNC formation is induced upon loss of KA120 and the MAC is required for *ka120*-dependent autoimmune activation, we propose that the MDNC may be a previously uncharacterized immune-activating subnuclear structure whose formation is tightly regulated by KA120 to prevent autoimmunity.

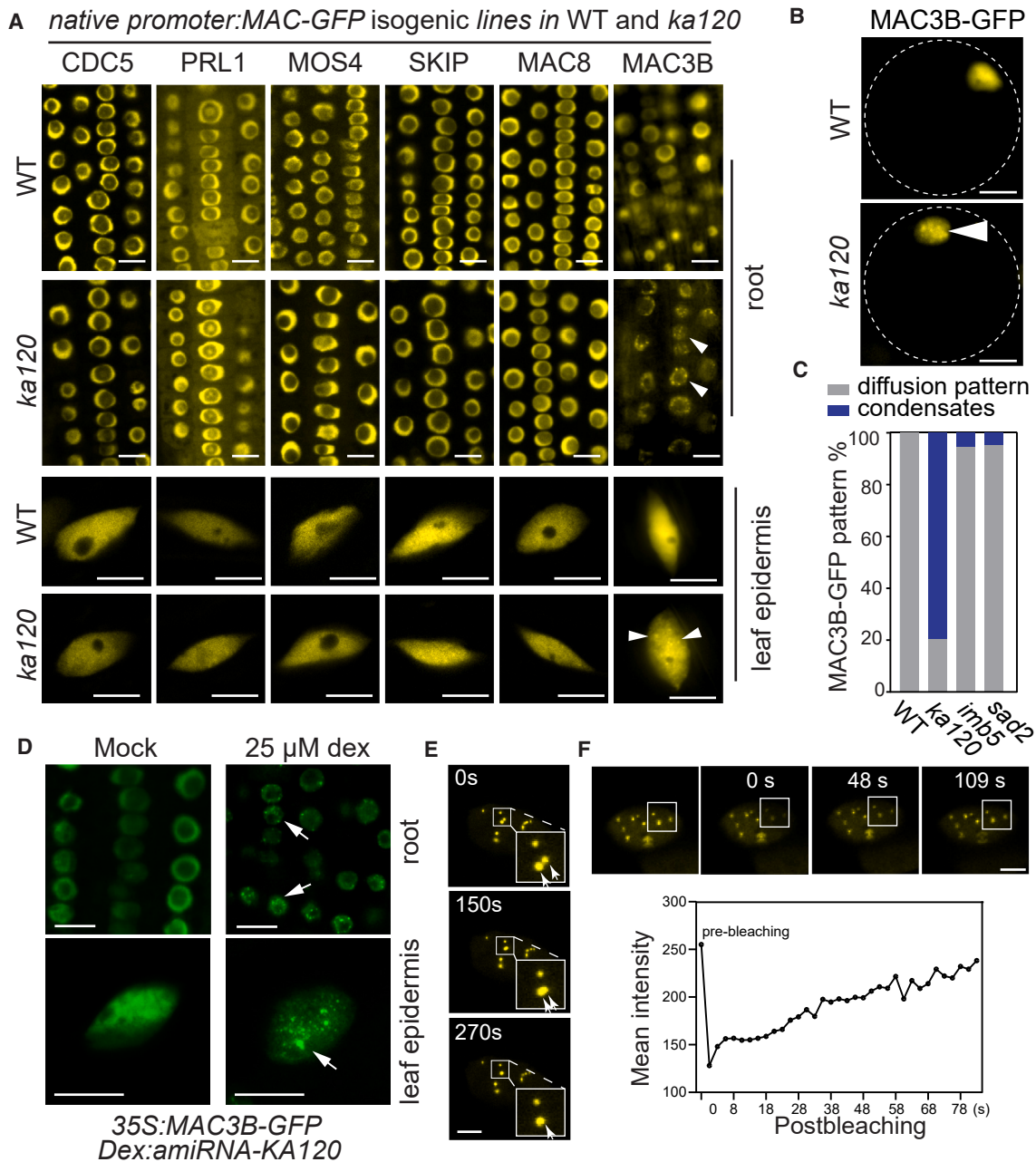


Figure 2. MAC3B forms nuclear condensates in the absence of KA120

(A) Subcellular localization of MAC proteins in root cells of WT and *ka120* plants. Native promoter-driven MAC-GFP constructs were transformed into *ka120* heterozygous plants, and isogenic WT and *ka120* lines were obtained for imaging in the T2 segregating population. Arrowheads indicate nuclear condensates. Scale bars, 10 μ m.

(B) Transient expression of MAC3B-GFP in WT and *ka120* protoplasts. Scale bars, 10 μ m.

(C) Quantification of the MAC3B-GFP nuclear condensate formation when transiently expressed in different mutant backgrounds (WT, $n = 204$; *ka120*, $n = 132$; *imb5*, $n = 222$; *sad2*, $n = 428$). Similar results were obtained twice.

(D) Inducible formation of MAC3B-GFP nuclear condensates when KA120 is transiently knocked down. The 35S:MAC3B-GFP line in the WT background was transformed with a dexamethasone-inducible promoter-driven artificial microRNA construct targeting KA120. The double transgenic line was treated with 25 μ M dex or water (mock) for 12 h before images were taken in root and leaf epidermal cells. Arrows indicate nuclear condensates. Scale bars, 10 μ m.

(E) Time-lapse microscopy showing fusion dynamics of MDNCs in 35S:MAC3B-GFP/Dex:amiRNA-KA120 plants treated with 25 μ M dex. Time 0 indicates the start of recording. Scale bars, 2 μ m.

(F) Fluorescence recovery after photobleaching (FRAP) using the same tissue as in (E). Nuclei were imaged and boxes indicate photobleaching area. Fluorescence images and fluorescence quantification were shown for two independent FRAP analyses. Time 0 indicates the start of photobleaching. Scale bars, 2 μ m. See also Figure S2.

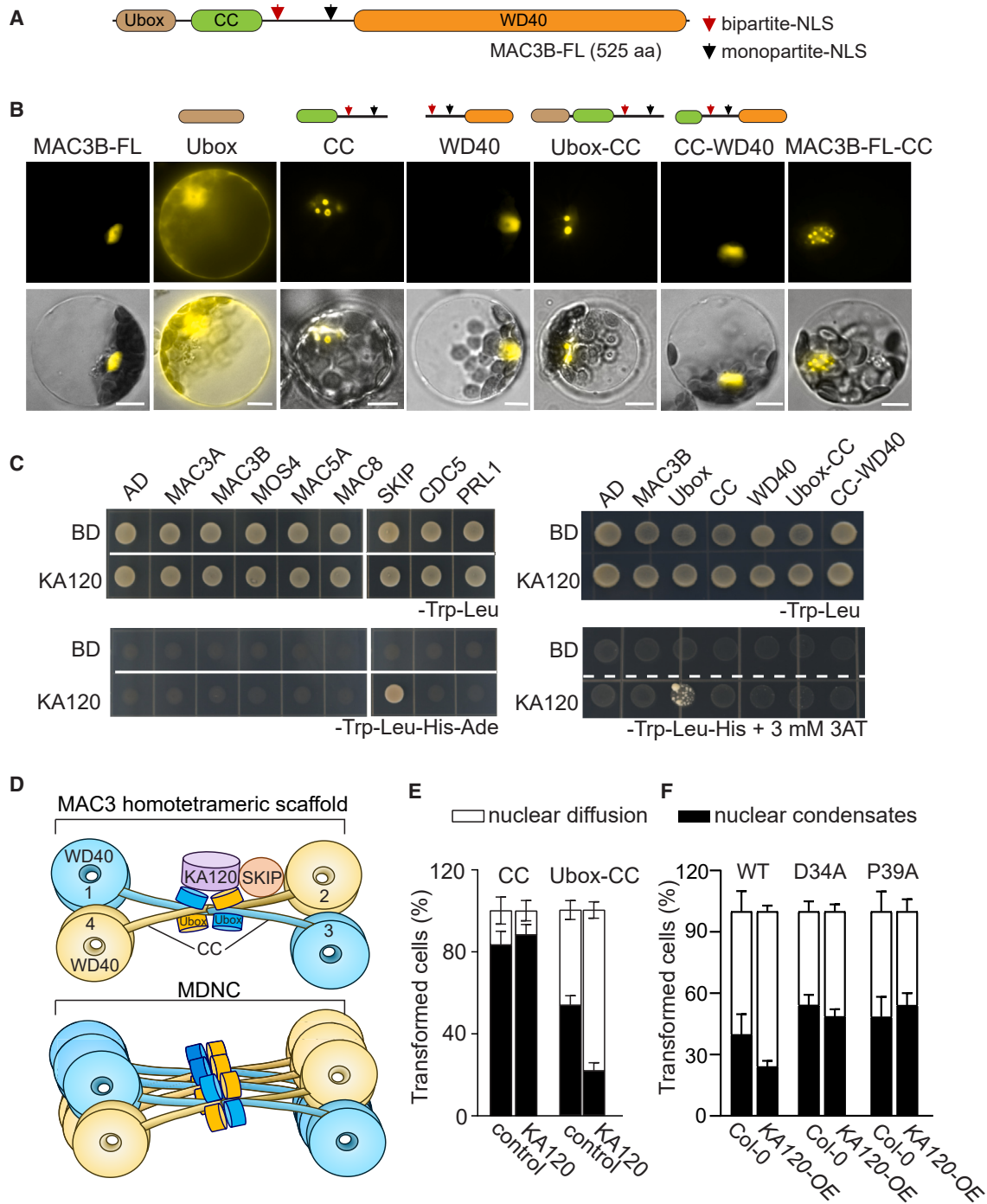


Figure 3. KA120 directly interacts with MAC proteins to prevent MDNC formation

(A) A schematic diagram of the *Arabidopsis* MAC3B protein domain structure. Predicted nuclear localization signals (NLSs) are shown by arrows.

(B) Transient expression of GFP-tagged full-length (FL) MAC3B, its three individual domains, and domain combinations in WT *Arabidopsis* protoplasts. Scale bars, 10 μ m.

(C) Y2H analysis using KA120 as the prey and different MAC proteins (left panel) and MAC3 domains (right panel) as the bait. Zygote yeasts were grown on double dropout medium (SD/-Leu-Trp), triple dropout medium (SD/-Leu-Trp-His)+3AT, or quadruple dropout medium (SD/-Leu-Trp-His-Ade) media. Empty vectors were used as negative controls.

(D) A schematic diagram showing the proposed chaperoning function of KA120. KA120 directly interacts with SKIP to associate with the MAC. The weak interaction between KA120 and the MAC3 U-box domain may affect U-box interaction with the adjacent CC domain and prevent the CC-driven condensation.

(legend continued on next page)

Direct interaction between KA120 and MAC contributes to suppression of MDNC formation

As the core scaffold of the complex, *Arabidopsis* MAC3 and human/yeast Prp19 share high sequence similarity (Figure S3A) and possess conserved domains (Figure 3A), including an N-terminal U-box domain for substrate ubiquitination, a CC domain for structural assembly, and a C-terminal WD40 domain for substrate recognition.³⁵

To investigate the mechanism behind MDNC formation, we first performed a truncational analysis by fusing GFP to different domains of MAC3B, including U-box, CC, WD40, U-box-CC, and CC-WD40, and transiently expressed these constructs in WT *Arabidopsis* protoplasts (Figure 3B). Consistent with our observation in transgenic plants, the full-length (FL) MAC3B is evenly distributed in the nucleus upon transient expression. The U-box domain alone cannot form condensates. However, the CC domain itself is sufficient to promote the spontaneous formation of nuclear condensates, and U-box-CC can also form nuclear condensates. We also fused an additional CC domain to the C terminus of the FL MAC3B and found that it could drive spontaneous formation of MAC3B condensates. These data support that the CC domain comprises a main structural basis for MDNC formation. Neither the WD40 nor the CC-WD40 is able to promote the formation of spontaneous condensates, suggesting that the WD40 domain may inhibit CC-mediated condensation, possibly by substrate recruitment.

To determine whether KA120 is directly involved in preventing the MDNC formation, we first tested whether there is a direct interaction between KA120 and the MAC by screening interactions between KA120 and MAC proteins using yeast-two-hybrid (Y2H). We found that KA120 showed a robust interaction with SKIP but not with other MAC proteins tested (Figure 3C). This result is supported by a predicted protein-protein interaction by AlphaFold-Multimer, which identified four potential salt bridges between KA120 and SKIP (Figure S3B). Although KA120 does not interact with the FL MAC3B in yeasts, KA120 displays a weak association with the truncated U-box domain (Figure 3C). Considering the well-established interaction between the U-box and the CC domain of Prp19,³⁶ we speculate that KA120's association with SKIP promotes its engagement with the MAC3 U-box domain, and this association contributes to MAC3's structural stability by reducing the exposure and condensation propensity of the adjacent CC domain (Figure 3D).

To validate this hypothesis and determine the direct role of KA120 in regulating MAC3 condensation, we co-overexpressed KA120-mCherry with MAC3B CC or U-box-CC domain in protoplasts. Intriguingly, we found that KA120 was able to inhibit over 60% of nuclear condensates formed by U-box-CC (Figure 3E), supporting the direct participation of KA120 in preventing MDNC formation. However, condensates formed by the CC

domain alone were not affected by KA120 overexpression. This result strongly supports our hypothesis that the stabilization of the MAC by KA120 requires KA120's association with the U-box domain of MAC3. To further substantiate this hypothesis, we used AlphaFold-Multimer to predict the interaction surface between MAC3 and KA120 and found that the conserved D34 and P39 residues of MAC3 U-box domain may be critical for its interaction with KA120 (Figure S3C). We subsequently mutagenized the two residues individually and generated MAC3B^{D34A} and MAC3B^{P39A} constructs. Remarkably, we found that KA120 indeed failed to inhibit MDNC formed by the two MAC3B mutants (Figure 3F). A previous structural analysis showed that P39A but not D34A disrupts the structure folding of Prp19 U-box domain.³⁷ Nevertheless, even the well-folded MAC3B^{D34A} mutant significantly compromises U-box interaction with KA120, confirming the importance of the predicted residues for the MAC3-KA120 interaction. The loss of interaction with and regulation by KA120 found in the MAC3B^{D34A} mutant further supports that KA120 functions to inhibit MAC3 condensation in the nucleus via physical associations with its U-box domain.

Spontaneous MDNC formation is sufficient to activate defense gene expression

To determine whether the formation of MDNCs contributes to the autoimmune activation in *ka120* plants, we sought to induce MDNCs in WT plants. Based on the above results, the CC domain is the key to promote MDNC formation. A previous structural analysis of human Prp19 reported that two amino acid substitutions in the CC domain (Q79A/D83A) weaken the U-box and CC interaction and may promote the CC exposure.³⁶ We thus made equivalent mutations in MAC3B (Q77A/D81A, Figure S3A) and generated stable 35S:MAC3B^{Q77A/D81A}-GFP transgenic plants. Remarkably, we found that MAC3B^{Q77A/D81A} indeed promotes the constitutive formation of MDNCs in stable transgenic plants in WT background (Figure 4A). In contrast, a U-box mutant construct MAC3B^{H31A/D34A} did not show a similar effect.

Next, we performed RNA-seq analysis using 35S:MAC3B^{Q77A/D81A}-GFP transgenic plants. Interestingly, although 35S:MAC3B^{Q77A/D81A}-GFP transgenic plants did not show a typical autoimmune phenotype (Figure S4A), we identified 310 differentially expressed genes (DEGs, FC > 2 and p value < 0.05) compared with WT plants (Table S2, GEO: GSE224520). GO term analysis revealed that the 230 upregulated DEGs are significantly enriched in defense-related processes (Figure 4B). This result was further validated by reverse transcription-quantitative PCR (RT-qPCR) using three independent 35S:MAC3B^{Q77A/D81A}-GFP transgenic lines, and in all cases, defense marker genes were significantly upregulated compared with WT plants (Figure 4C).

(E) Quantification of nuclear condensate formation when transiently expressing GFP-tagged MAC3B CC or U-box-CC domain with or without KA120-mCherry coexpression in protoplasts (CC, n1 = 187, n2 = 121, n3 = 89; CC+KA120, n1 = 118, n2 = 109; U-box-CC, n1 = 168, n2 = 148, n3 = 90; U-box-CC+KA120, n1 = 153, n2 = 146, n3 = 168).

(F) Quantification of nuclear condensate formation when transiently expressing GFP-tagged MAC3B U-box-CC domain (WT, D34A, or P39A mutant form) in protoplasts prepared from Col-0 or KA120-mCherry overexpression (OE) plants (WT/Col-0: n1 = 58, n2 = 56, n3 = 55, n4 = 87; WT/KA120-OE: n1 = 47, n2 = 61, n3 = 54, n4 = 119; D34A/Col-0: n1 = 60, n2 = 58, n3 = 43; D34A/KA120-OE: n1 = 43, n2 = 43, n3 = 50, n4 = 56; P39A/Col-0: n1 = 51, n2 = 47, n3 = 55; P39A/KA120-OE: n1 = 54, n2 = 45, n3 = 59).

See also Figure S3.

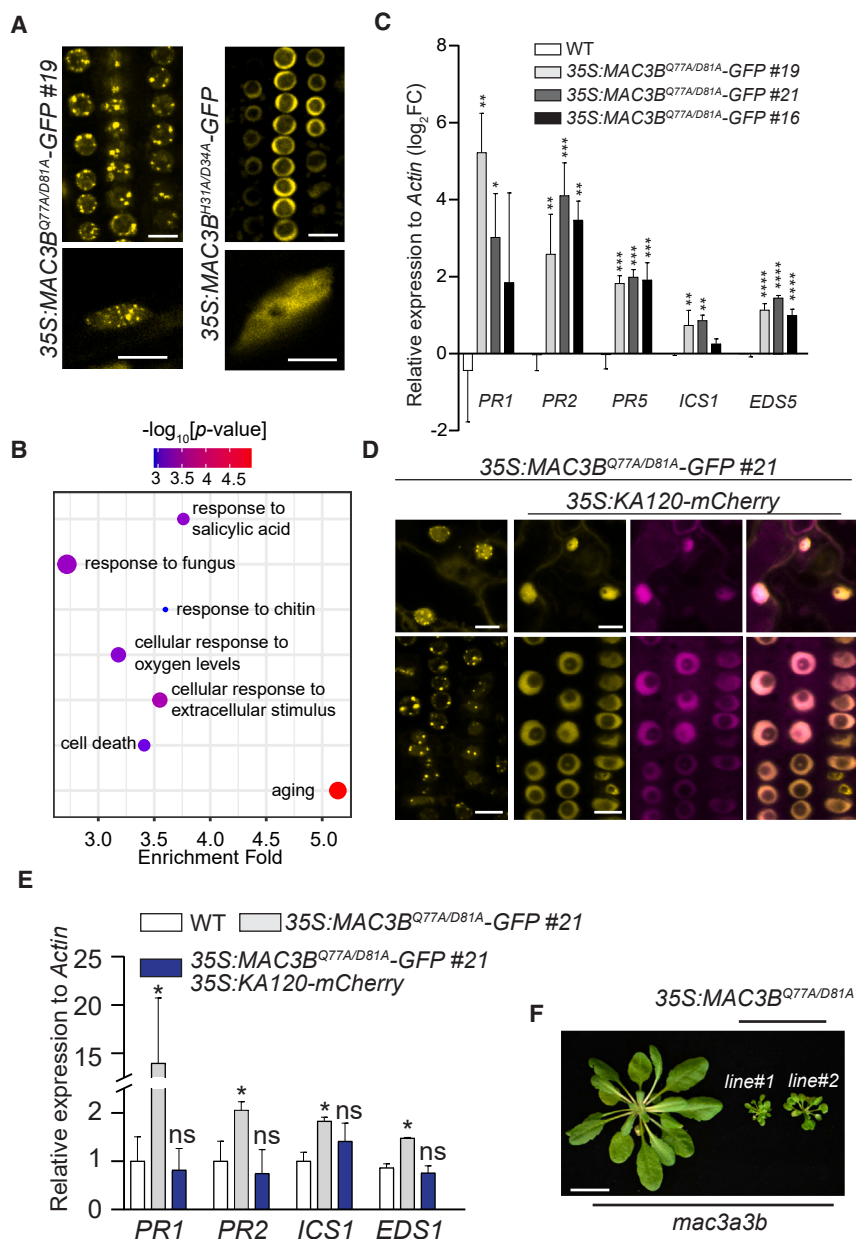


Figure 4. Formation of MAC3 condensates is sufficient to activate defense gene expression

(A) Subcellular localization of MAC3B mutants. Root cells of transgenic plants expressing *MAC3B^{Q77A/D81A}-GFP* and *MAC3B^{H31A/D34A}-GFP* in WT background. Scale bars, 10 μ m.

(B) GO term analysis of significantly upregulated genes identified in *35S:MAC3B^{Q77A/D81A}-GFP* transgenic plants compared with WT. Data were obtained by RNA-seq analysis using 7-day-old WT and *35S:MAC3B^{Q77A/D81A}-GFP* transgenic seedlings. Two biological replicates were used (GEO: GSE224520).

(C) The relative expression of defense marker genes measured by RT-qPCR in *35S:MAC3B^{Q77A/D81A}-GFP* lines. Data are presented as mean \pm SD (n = 2 biological replicates). Statistical analysis was performed using Student's t test (**p < 0.01; ***p < 0.001; ****p < 0.0001). WT plants served as control.

(D) Subcellular localization of *MAC3B^{Q77A/D81A}-GFP* in leaf cells (upper panel) and root cells (lower panel) of transgenic plants in WT and *35S:KA120-mCherry* backgrounds. Scale bars, 10 μ m.

(E) The relative expression of defense marker genes to *Actin* measured by RT-qPCR in WT, *35S:MAC3B^{Q77A/D81A}-GFP*, and *35S:MAC3B^{Q77A/D81A}-GFP/35S:KA120-mCherry* plants. Expression levels were normalized to that in WT. Data are presented as mean \pm SD (n = 3 biological replicates). Statistical analysis was performed using Student's t test (*p < 0.05; ns, not significant).

(F) Phenotype of overexpressing *MAC3B^{Q77A/D81A}-GFP* in the *mac3a mac3b* mutant background. 6-week-old soil-grown plants of two independent lines were shown. Scale bars, 2 cm. See also Figure S4 and Table S2.

To test whether KA120 can also inhibit the *MAC3B^{Q77A/D81A}* condensate formation, we crossed a *35S:KA120-mCherry* line with the *35S:MAC3B^{Q77A/D81A}-GFP* line. In the F2 segregating population, we found that progenies without KA120-mCherry expression showed clear MAC3B condensates, whereas those expressing KA120-Cherry were not able to form MAC3B condensates (Figure 4D). More importantly, we found that the inhibition of MAC3B condensation correlates with the suppression of defense gene expression in *35S:MAC3B^{Q77A/D81A}-GFP* plants (Figure 4E). These results support that the formation of MDNCs is sufficient to trigger defense gene expression and reinforce our hypothesis that KA120 functions as a necessary chaperoning factor to inhibit MDNC formation and prevent autoimmunity.

Remarkably, when we generated *35S:MAC3B^{Q77A/D81A}-GFP* transgenic plants in the *mac3a mac3b* double-mutant back-

ground, we found that more than half of the obtained *35S:MAC3B^{Q77A/D81A}-GFP* lines exhibited stunted growth, wrinkled leaves, and spontaneous cell death, similar to the *ka120* mutant (Figure 4F). Because Prp19 protein is known to form homotetramers for function,³⁶ we think that the previously observed mild autoimmune activation induced by *MAC3B^{Q77A/D81A}* in the WT background may be due to the endogenous expression of *MAC3A/3B* (Figure S4B), which forms autoinhibited heterotetramers with *MAC3B^{Q77A/D81A}*.

The canonical composition and function of the MAC are compromised in MDNCs

Knowing that MDNC contributes to immune activation, we next investigated how the MAC function may be altered upon condensation and how that change may contribute to MDNC-dependent immune activation. We generated isogenic *pMAC3B:MAC3B-TurboID* lines in WT and *ka120* background and subsequently profiled the composition of the MAC in the presence and absence of KA120, representing the soluble and condensate MAC, respectively. Transgenic plants in both backgrounds were treated with free biotin for proximity labeling (Figure S5A) and were then

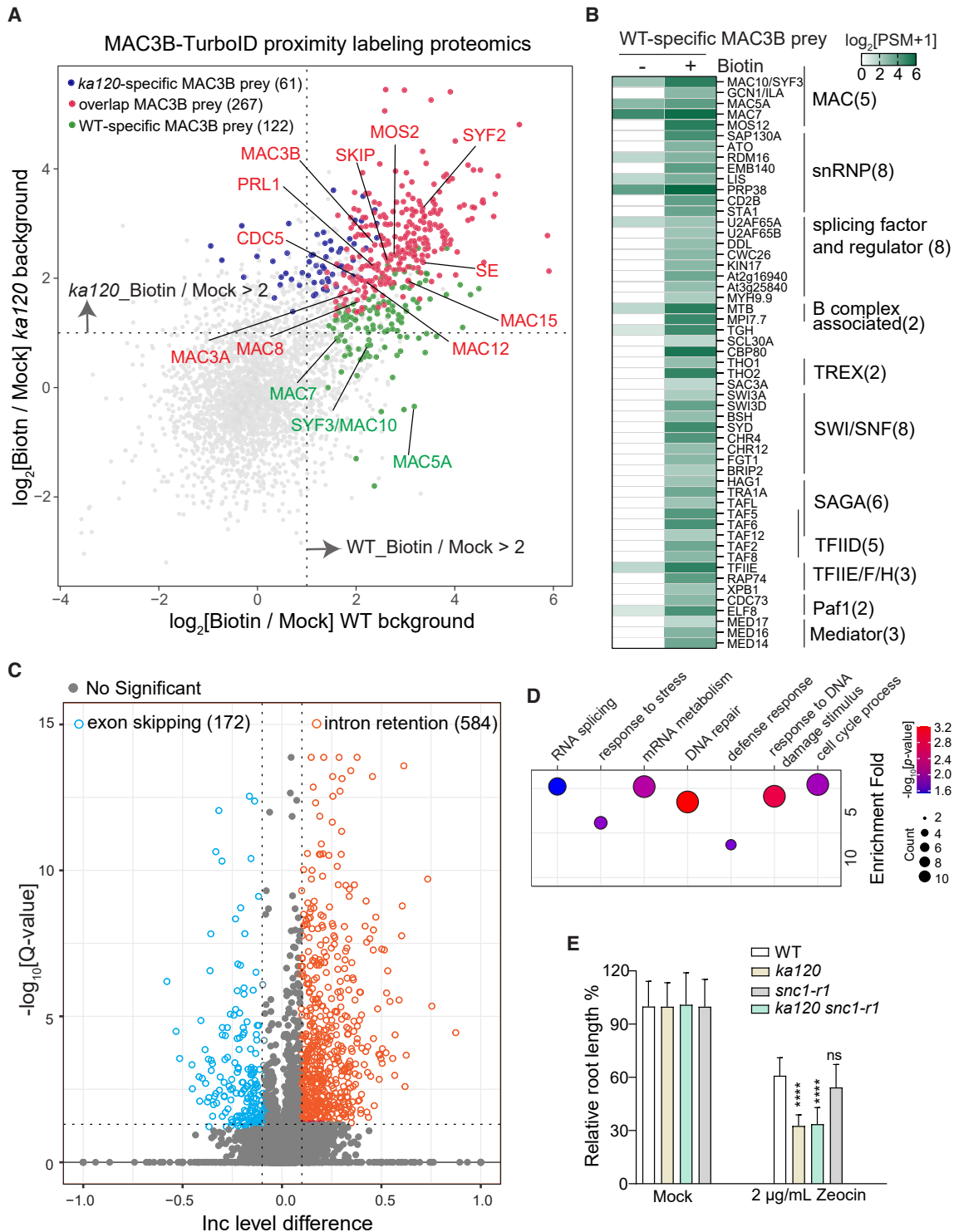


Figure 5. KA120 is required for maintaining the integrity and canonical function of the MAC

(A) Scatter plot showing significantly enriched proteins identified by proximity-labeling proteomics using *pMAC3B-MAC3B-TurboID-HA* transgenic plants in WT and *ka120* backgrounds. Plants were treated with or without biotin, and two biological replicates were used per treatment per background. MAC3B-specific preys in each background were selected using cutoff p value < 0.1 (linear model F tests, $n = 2$), fold-change > 2 , and PSM > 2 compared with mock-treated samples in corresponding background. Candidates that are specifically probed by MAC3B in *ka120* mutant plants and WT plants are labeled with blue and green dots, respectively. Overlapping candidates of the two samples are labeled with red dots. Proteins that are not significantly enriched in either sample are represented as gray dots.

(legend continued on next page)

subjected to LFQMS analysis. The MAC3B proximiome in WT (representing canonical MAC) and *ka120* mutant (representing MDNCs) was selected by comparing with water (mock)-treated samples in the corresponding background using cutoff $FC > 2$, p value < 0.1 , and $PSM > 2$ (Table S3, ProteomeXchange: PXD040403). Comparative analysis of the two MAC3B proximiomes revealed that a number of MAC components, including MAC5A, MAC7, and SYF3/MAC10, are no longer associated with MAC3B in the *ka120* mutant, or their association is largely compromised (Figures 5A and 5B). This result suggests that the MAC integrity is disrupted or compositionally altered in MDNCs. Supporting the compromised MAC integrity in *ka120*, many snRNPs and splicing factors and regulators were probed by MAC3B in WT but not in *ka120* plants (Figures 5B and S5B). Chromatin remodelers, transcription initiator factor II (TFII) proteins, and key transcription coactivators such as the mediator complex, and the SAGA complex components were identified by MAC3B in WT (Figure 5B), likely reflecting the coupled transcription and mRNA splicing process. However, those factors are also mostly absent in the MAC3B proximiome in *ka120* plants.

The two major canonical functions of the MAC are mRNA splicing and DNA repair. Supporting a generally disrupted function of the MAC in *ka120*, we found 584 intron retention events and 172 exon skipping events in the *ka120* mutant using RNA-seq analysis (Figure 5C; Table S4). Notably, GO analysis indicates that these dysregulated splicing events mainly affect genes that function in mRNA splicing, DNA repair, and DNA damage responses (Figure 5D). We think this enrichment is likely caused by compensatory upregulation of these genes in *ka120* plants and subsequent mis-splicing of their mRNAs due to the malfunction of the MAC. A similar defect in mRNA splicing and processing was found in *35S:MAC3B^{Q77A/D81A}-GFP* transgenic plants (Figures S5C and S5D; Table S5). Furthermore, compared with WT, the *ka120* mutant is significantly more sensitive to zeocin, a reagent that causes DNA double-strand breaks (Figure 5E), suggesting compromised DNA repair. These results together support the conclusion that KA120 is required for maintaining the canonical function of the MAC.

It is noteworthy that the enhanced zeocin sensitivity of *ka120* cannot be suppressed by *snc1-r1* (Figure 5E), which was previously shown to suppress the autoimmune activation in *ka120*.²⁴ Similarly, the *pad4* mutant cannot suppress RNA splicing defects in *ka120* (Figure S5E). These results indicate that defects in the canonical function of the MAC cannot explain the MDNC-mediated autoimmune activation in *ka120*.

MDNCs contain negative immune regulators that genetically interact with KA120

Although compromised in the canonical MAC composition and function, MDNCs appear to gain association with other

components. There are 61 proteins probed specifically by MAC3B in *ka120* but not in WT plants (Figure 5A). Among them, at least 7 proteins have been reported to directly participate in the regulation of plant immunity (Table S6). To validate their contributions to *ka120*-dependent immune activation, we obtained T-DNA insertion mutants of the 7 genes and crossed them with *ka120*. Interestingly, we found that mutations in *IRR* and *JAO2* could significantly enhance the *ka120* phenotype, although the *irr* and *jao2* single mutant did not show observable phenotypes (Figures 6A and 6B). *IRR* is an RNA-binding protein (RBPs) that regulates alternative splicing of *CPK28*, a key negative regulator of PTI,³⁸ and *JAO2* was shown to negatively regulate JA-mediated defense by catalyzing the oxidation of JA.³⁹ The observed genetic interaction indicates that *IRR/JAO2* contributes to the suppression of *ka120*-induced autoimmunity. One hypothesis is that in the *ka120* mutant, *IRR* and *JAO2* are partially recruited to the MDNC, where their immune-repressing function was blocked, which contributes to defense activation. Complete loss of *IRR/JAO2* could further enhance this effect in the *irr ka120* and *jao2 ka120* double mutants. Double mutant of *ka120* with the other 5 genes did not alter *ka120* phenotypes (Figure S6A). This is possibly due to the presence of functionally redundant homologs; however, it is more likely that the MDNC-dependent immune activation requires simultaneous recruitment of multiple negative immune regulators.

Taken together, the results above provide support for the hypothesis that MDNCs are immune-promoting subnuclear condensates. It is plausible that MDNCs are capable of recruiting negative immune regulatory proteins such as *IRR* and *JAO2*, which may contribute to the activation of plant immune responses.

Pathogen-induced immune activation promotes MDNC formation

To determine whether MDNCs are induced by pathogen-triggered immune activation, we inoculated *35S:MAC3B-GFP* plants with the bacterial pathogen *Pseudomonas syringae* (*Pst*) DC3000. We found that MDNCs could be robustly induced by both the virulent *Pst*DC3000 strain and the avirulent *Pst*DC3000:AvrRps4 strain in leaf cells (Figure 6C). Similar results could be obtained using native promoter-driven *SKIP-GFP* and *PRL1-GFP* transgenic plants (Figure S6B). These results support that the MDNC formation is tightly associated with and may play a role in pathogen-induced immune activation. However, when we compared KA120 protein levels before and after pathogen infection, we did not observe significant changes, suggesting that pathogen infection may affect the activity rather than the protein level of KA120 to promote the MDNC formation (Figure S6C).

(B) Heatmap showing normalized PSM values of significant protein and protein complexes probed by MAC3B-TurboID in WT but not *ka120* transgenic plants.

(C) Intron retention and exon skipping events identified in the *ka120* mutant ($FDR < 0.05$ and absolute $\ln(\text{LevelDifference}) > 0.1$). Data were obtained by re-analyzing our previous RNA-seq data using 3-week-old rosette leaves (GEO: GSE147682).

(D) GO analysis of mis-spliced genes in the *ka120* mutant. Representative GO terms are shown.

(E) Measurement of plant response to DNA damage inducing reagent zeocin. Plants were grown on 1/2 MS media supplied with or without 2 $\mu\text{g}/\text{mL}$ zeocin for 7 days. The root length of zeocin-treated samples was normalized to mock-treated samples. Statistical analysis was performed using Student's *t* test (**** $p < 0.0001$; ns, not significant).

See also Figure S5 and Tables S3, S4, and S5.

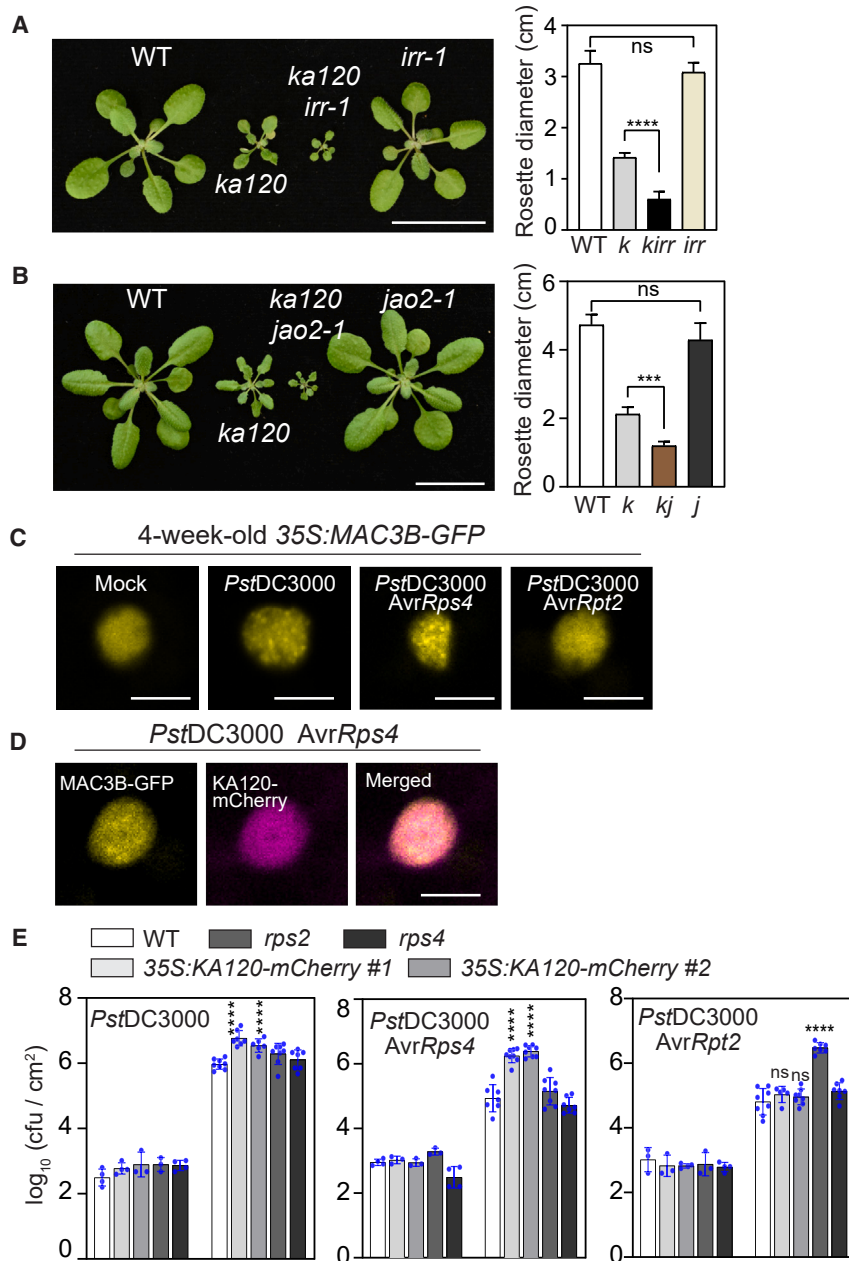


Figure 6. MAC condensates are induced by pathogen infection and contain negative immune regulators that genetically interact with KA120

(A and B) 3-week-old soil-grown WT, *ka120*, *irr*, and *ka120 irr* double-mutant plants (A), and 4-week-old soil-grown WT, *ka120*, *jao2-1*, and *ka120 jao2* double-mutant plants (B). The rosette diameter was measured. Data are presented as mean \pm SD ($n = 7$). Statistical analysis was performed using Student's *t* test (** $p < 0.001$; ns, not significant). Scale bars, 2 cm.

(C) Induction of MDNCs in 35S:MAC3B-GFP transgenic plants infected with the bacterial pathogen *Pseudomonas syringae* DC3000 virulent strain ($OD_{600} = 0.01$) and avirulent strains carrying effector AvrRps4 or AvrRps2 ($OD_{600} = 0.01$). Nuclei of leaf mesophyll cells of 4-week-old plants were shown.

(D) A representative nucleus of 35S:MAC3B-GFP/35S:KA120-mCherry double transgenic plants infected by *Pst*DC3000:AvrRps4. Images in (C) and (D) were taken 20~24 h past infection. Scale bars, 5 μ m.

(E) Growth of *Pst*DC3000 and *Pst*DC3000:AvrRps4/AvrRpt2 on two independent 35S:KA120-mCherry lines (homozygous T3 plants were used). WT, *rps2*, and *rps4-2* mutants were used as control. Note that the *rps4-2* mutant displays susceptibility to *Pst*/AvrRps4 at 24°C but not at 22°C. The growth of bacteria was counted at 3 days after infection, and plants were incubated under 22°C. Data are presented as mean \pm SD for six biological replicates. Student's *t* tests were performed (**** $p < 0.0001$; ns, not significant). CFU, colony forming unit. See also Figure S6 and Table S6.

DISCUSSION

Our study supports a model in which KA120 associates with the MAC in the nucleus via its physical interaction with SKIP/MAC6. We propose that SKIP may bring KA120 in proximal to the U-box domain of MAC3, which helps to substantiate the interaction between the two. This consequently inhibits the exposure and reduces the condensation propensity of the CC domain of MAC3 to prevent MDNC formation. KA120-dependent prevention of

Remarkably, the pathogen-induced MDNC formation can be completely suppressed by overexpressing KA120 in 35S:MAC3B-GFP/35S:KA120-mCherry double transgenic plants (Figure 6D), reinforcing the previous finding that KA120 is able to suppress MAC3B condensation and immune activation. In line with those observations, KA120 overexpression lines display significantly enhanced susceptibility to both *Pst*DC3000 and *Pst*DC3000:AvrRps4 (Figure 6E), supporting that MDNCs contribute to plant immune induction. Curiously, MDNCs were barely induced by *Pst*DC3000:AvrRpt2, and consistently, KA120 overexpression lines are not more susceptible to *Pst*DC3000:AvrRpt2 compared with WT. These data suggest that MDNCs are selectively induced by certain immune signaling pathways.

MAC3 condensation is required for the canonical mRNA splicing and DNA repair function of the MAC in the nucleus. However, upon pathogen-induced immune activation, at least a portion of MAC3 protein is structurally destabilized due to dissociation from KA120 and undergoes condensation to form MDNCs, although it is not clear what triggers the dissociation of KA120 from the MAC (Figure 7). Nonetheless, formation of MDNCs contributes to defense gene expression, possibly through recruiting and deactivating negative immune regulators. Below, we highlight a few intriguing concepts derived from this model:

First, KA120, a conserved karyopherin- β , plays an unexpected role in regulating biomolecular condensation of its substrates in plants. Several recent breakthrough reports showed that human

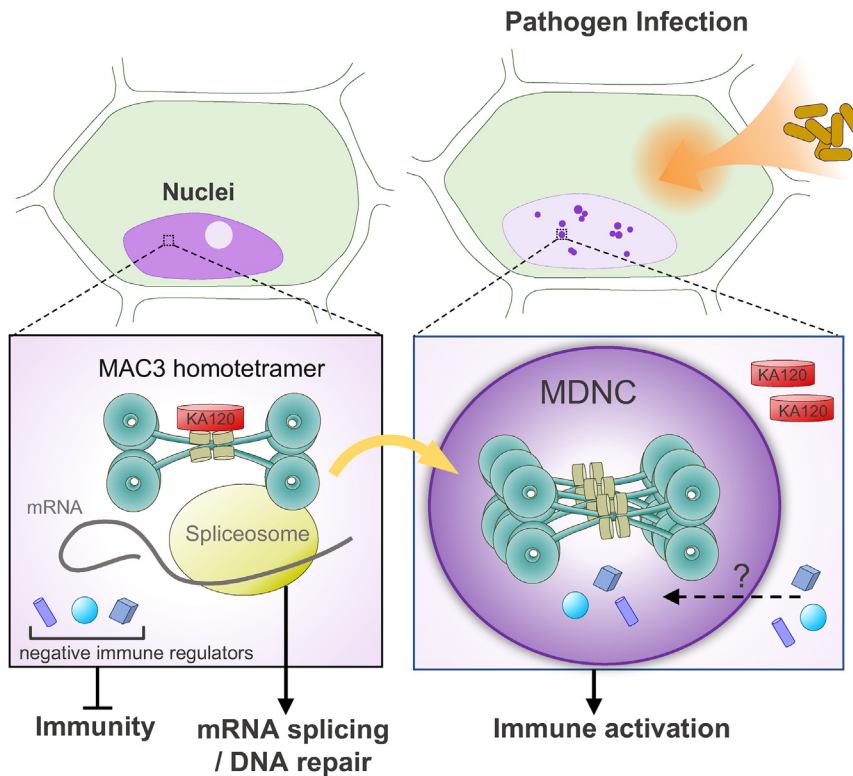


Figure 7. Working model for MDNC-mediated immune activation

KA120 associates with the MAC in the nucleus through physical interactions with MAC proteins. This association is critical for maintaining the canonical mRNA splicing and DNA repair function of the MAC, as it brings KA120 in proximity to the U-box domain of MAC3 and stabilizes the adjacent CC domain, thereby reducing the propensity for MAC3 condensation. However, upon pathogen-induced immune activation, MAC3 protein undergoes structural destabilization due to dissociation from KA120 and condenses via the CC domain to form MDNCs in the nucleus. The dissociation mechanism of KA120 from the MAC is not yet fully understood. The formation of MDNCs contributes to defense activation, potentially by promoting the phase transition and sequestration of negative immune regulators in MDNCs.

not overlap with well-characterized nuclear bodies nor its components have been reported in other immune-inducible nuclear condensates.^{33,44} Unlike many previously reported nuclear condensates in plants, which enhance protein or protein complex activities by increasing their concentration,^{33,45–47} MDNCs seem to

karyopherin- β 2, a homolog of IMB2 in *Arabidopsis*, participates in preventing and reverting aberrant and pathological phase separation of RBPs that lead to neurodegenerative diseases.^{40–43} Karyopherin- β 2 does so by recognizing RBPs' PY (proline-tyrosine)-nuclear localization signal (NLS) and binding weakly with multiple other regions to disrupt the protein aggregates. However, it is unclear if this function is conserved in other eukaryotic species and if other karyopherin- β s have similar activities. Our findings indicate that plant karyopherin- β s may have evolved or, more likely, preserve a similar function in regulating biomolecular condensation. However, KA120 resolves MDNCs in the nucleus, whereas karyopherin- β 2 reverts RBP aggregates in the cytosol. Given that MAC3 and KA120 are both evolutionarily conserved proteins, it would be interesting to determine whether human KA120 regulates the phase transition of Prp19, and if so, what is the functional significance of it in humans.

Second, the karyopherin- β family proteins regulate communications between subcellular compartments and were established before the last eukaryotic common ancestor. LLPS is likely an even more ancient biophysical mechanism that mediates cellular compartmentalization. Interestingly, karyopherin- β s mediate nuclear transport by interacting extensively with an LLPS environment established by the selective barrier inside the nuclear pore. Thus, the interplay between karyopherin- β and biomolecular condensates raises intriguing questions about the evolution of the nucleocytoplasmic transport system. In this sense, the function of karyopherins in reverting biomolecular condensates might have evolved earlier than its nuclear transporting activity.

Third, the MDNC appears to be a previously uncharacterized type of immune-related biomolecular condensate, which does

lose the canonical splicing and DNA repair activity due to the partial disassembly of the MAC and its disassociation with other mRNA processing machinery. Instead, MDNCs appear to “gain functions” by recruiting and possibly sequestering negative immune regulators, including IRR and JAO2, to activate defense, although how the specific recruitment is achieved remains unclear. Also, we cannot rule out the possibility that MDNCs recruit positive immune regulators for their activation.

We showed before that the *ka120* mutant exhibits a transcriptional signature that resembles the Toll/interleukin-1 receptor (TIR)-type NLR immune receptor (TNL) RPS4-mediated but not elf18-induced immune activation. In addition, mutations in classical TNL signaling components including *PAD4* and *EDS1* as well as the TNL gene *SNC1* can largely suppress the *ka120* phenotype. Moreover, KA120 overexpression can almost fully rescue the *SNC1*-mediated autoimmune phenotype.²⁴ Here, we showed that *mac* mutants can suppress both *ka120*- and *SNC1*-mediated immune activation. Taken together, we think that KA120, MDNC, and *SNC1* may work in the same pathway to regulate plant immune activation, particularly the TNL-mediated immunity. In line with this idea, *mac3a mac3b* suppresses the *ka120* phenotype to a similar extent to the *snc1-r1* mutant, and the suppression is not further enhanced by the *mac3a mac3b snc1-r1* triple mutant. It is possible that upon PTI/ETI induction, *SNC1* activation promotes the MDNC formation and functions upstream of it; however, we did not observe constitutive MDNC formation in the *snc1-1* autoactive mutant. Alternatively, *SNC1* may be recruited to MDNCs for activation or recognize MDNC directly or indirectly to activate. In both cases, MDNC components are required for *SNC1*-dependent immune activation. KA120

affects the cellular dynamics of both MAC and SNC1 and appears to function upstream of both.

STAR★METHODS

Detailed methods are provided in the online version of this paper and include the following:

- **KEY RESOURCES TABLE**
- **RESOURCE AVAILABILITY**
 - Lead contact
 - Materials availability
 - Data and code availability
- **EXPERIMENTAL MODEL AND STUDY PARTICIPANT DETAILS**
 - Plants
 - Microbe strains
- **METHOD DETAILS**
 - Plasmid construction
 - Protoplast transfection
 - RNA extraction and RT-qPCR
 - Pathogen infection
 - Drug treatment
 - Yeast two hybrid
 - FRAP analysis
 - Proximity labeling proteomics
 - RNA-seq
 - Protein structure prediction
- **QUANTIFICATION AND STATISTICAL ANALYSIS**
 - Statistical analysis
 - Proximity labeling proteomics analysis
 - RNA-seq analysis
 - Alternative splicing analysis

SUPPLEMENTAL INFORMATION

Supplemental information can be found online at <https://doi.org/10.1016/j.chom.2023.08.015>.

ACKNOWLEDGMENTS

We thank Dr. Jennifer Lewis from the USDA Plant Gene Expression Center for providing the *zin1* mutant, ZIN1 DNA construct, and the *rps4-2* mutant. We also thank the supercomputing platform at the National Key Laboratory of Crop Improvement for Stress Tolerance and Production for providing computational resources. This project was supported by the USDA National Institute of Food and Agriculture (HATCH project CA-B-PLB-0243-H), National Science Foundation (NSF-MCB 2049931), Hellman Fellows Fund, and startup funds from the Innovative Genomics Institute (IGI) and the University of California, Berkeley (to Y.G.).

AUTHOR CONTRIBUTIONS

M.J. and Y.G. designed the research. X.C. analyzed RNA-seq and proteomic data. X.S. performed KA120 proximity-labeling proteomics experiments. Y.F. performed the AlphaFold-Multimer prediction. M.J. performed all the rest of the experiments. M.J. and Y.G. wrote the paper, and all authors discussed and edited the paper.

DECLARATION OF INTERESTS

The authors declare no competing interests.

Received: February 27, 2023

Revised: July 7, 2023

Accepted: August 21, 2023

Published: September 14, 2023

REFERENCES

1. Zhou, J.M., and Zhang, Y. (2020). Plant immunity: danger perception and signaling. *Cell* 181, 978–989. <https://doi.org/10.1016/j.cell.2020.04.028>.
2. Lapin, D., Johannndrees, O., Wu, Z., Li, X., and Parker, J.E. (2022). Molecular innovations in plant TIR-based immunity signaling. *Plant Cell* 34, 1479–1496. <https://doi.org/10.1093/plcell/koac035>.
3. Ngou, B.P.M., Ding, P., and Jones, J.D.G. (2022). Thirty years of resistance: zig-zag through the plant immune system. *Plant Cell* 34, 1447–1478. <https://doi.org/10.1093/plcell/koac041>.
4. Yuan, M., Jiang, Z., Bi, G., Nomura, K., Liu, M., Wang, Y., Cai, B., Zhou, J.M., He, S.Y., and Xin, X.F. (2021). Pattern-recognition receptors are required for NLR-mediated plant immunity. *Nature* 592, 105–109. <https://doi.org/10.1038/s41586-021-03316-6>.
5. Ngou, B.P.M., Ahn, H.K., Ding, P., and Jones, J.D.G. (2021). Mutual potentiation of plant immunity by cell-surface and intracellular receptors. *Nature* 592, 110–115. <https://doi.org/10.1038/s41586-021-03315-7>.
6. Zhang, J., Coaker, G., Zhou, J.M., and Dong, X. (2020). Plant immune mechanisms: from reductionistic to holistic points of view. *Mol. Plant* 13, 1358–1378. <https://doi.org/10.1016/j.molp.2020.09.007>.
7. Gu, Y., Zavaliev, R., and Dong, X. (2017). Membrane trafficking in plant immunity. *Mol. Plant* 10, 1026–1034. <https://doi.org/10.1016/j.molp.2017.07.001>.
8. Lu, H., McClung, C.R., and Zhang, C. (2017). Tick Tock: circadian regulation of plant innate immunity. *Annu. Rev. Phytopathol.* 55, 287–311. <https://doi.org/10.1146/annurev-phyto-080516-035451>.
9. Wang, W., and Gu, Y. (2022). The emerging role of biomolecular condensates in plant immunity. *Plant Cell* 34, 1568–1572. <https://doi.org/10.1093/plcell/koab240>.
10. Pieterse, C.M., Van der Does, D., Zamioudis, C., Leon-Reyes, A., and Van Wees, S.C. (2012). Hormonal modulation of plant immunity. *Annu. Rev. Cell Dev. Biol.* 28, 489–521. <https://doi.org/10.1146/annurev-cellbio-092910-154055>.
11. Fang, Y., and Gu, Y. (2021). Regulation of plant immunity by nuclear membrane-associated mechanisms. *Front. Immunol.* 12, 771065. <https://doi.org/10.3389/fimmu.2021.771065>.
12. Monaghan, J., Xu, F., Gao, M., Zhao, Q., Palma, K., Long, C., Chen, S., Zhang, Y., and Li, X. (2009). Two Prp19-like U-box proteins in the MOS4-associated complex play redundant roles in plant innate immunity. *PLoS Pathog.* 5, e1000526. <https://doi.org/10.1371/journal.ppat.1000526>.
13. Palma, K., Zhao, Q., Cheng, Y.T., Bi, D., Monaghan, J., Cheng, W., Zhang, Y., and Li, X. (2007). Regulation of plant innate immunity by three proteins in a complex conserved across the plant and animal kingdoms. *Genes Dev.* 21, 1484–1493. <https://doi.org/10.1101/gad.1559607>.
14. Makarova, O.V., Makarov, E.M., Urlaub, H., Will, C.L., Gentzel, M., Wilm, M., and Lührmann, R. (2004). A subset of human 35S U5 proteins, including Prp19, function prior to catalytic step 1 of splicing. *EMBO J.* 23, 2381–2391. <https://doi.org/10.1038/sj.emboj.7600241>.
15. Song, E.J., Werner, S.L., Neubauer, J., Stegmeier, F., Aspden, J., Rio, D., Harper, J.W., Elledge, S.J., Kirschner, M.W., and Rape, M. (2010). The Prp19 complex and the Usp4Sart3 deubiquitinating enzyme control reversible ubiquitination at the spliceosome. *Genes Dev.* 24, 1434–1447. <https://doi.org/10.1101/gad.1925010>.
16. Maréchal, A., Li, J.M., Ji, X.Y., Wu, C.S., Yazinski, S.A., Nguyen, H.D., Liu, S., Jiménez, A.E., Jin, J., and Zou, L. (2014). PRP19 transforms into a sensor of RPA-ssDNA after DNA damage and drives ATR activation via a ubiquitin-mediated circuitry. *Mol. Cell* 53, 235–246. <https://doi.org/10.1016/j.molcel.2013.11.002>.

17. Idrissou, M., and Maréchal, A. (2022). The PRP19 ubiquitin ligase, standing at the cross-roads of mRNA processing and genome stability. *Cancers (Basel)* *14*, 878. <https://doi.org/10.3390/cancers14040878>.
18. Monaghan, J., Xu, F., Xu, S., Zhang, Y., and Li, X. (2010). Two putative RNA-binding proteins function with unequal genetic redundancy in the MOS4-associated complex. *Plant Physiol.* *154*, 1783–1793. <https://doi.org/10.1104/pp.110.158931>.
19. Xu, F., Xu, S., Wiermer, M., Zhang, Y., and Li, X. (2012). The cyclin L homolog MOS12 and the MOS4-associated complex are required for the proper splicing of plant resistance genes. *Plant J.* *70*, 916–928. <https://doi.org/10.1111/j.1365-3113X.2012.04906.x>.
20. van Wersch, R., Li, X., and Zhang, Y. (2016). Mighty dwarfs: Arabidopsis autoimmune mutants and their usages in genetic dissection of plant immunity. *Front. Plant Sci.* *7*, 1717. <https://doi.org/10.3389/fpls.2016.01717>.
21. Freh, M., Gao, J., Petersen, M., and Panstruga, R. (2022). Plant autoimmunity—fresh insights into an old phenomenon. *Plant Physiol.* *188*, 1419–1434. <https://doi.org/10.1093/plphys/kiab590>.
22. Li, X., and Gu, Y. (2020). Structural and functional insight into the nuclear pore complex and nuclear transport receptors in plant stress signaling. *Curr. Opin. Plant Biol.* *58*, 60–68. <https://doi.org/10.1016/j.pbi.2020.10.006>.
23. Xu, F., Jia, M., Li, X., Tang, Y., Jiang, K., Bao, J., and Gu, Y. (2021). Exportin-4 coordinates nuclear shuttling of TOPLESS family transcription corepressors to regulate plant immunity. *Plant Cell* *33*, 697–713. <https://doi.org/10.1093/plcell/koaa047>.
24. Jia, M., Shen, X., Tang, Y., Shi, X., and Gu, Y. (2021). A karyopherin constrains nuclear activity of the NLR protein SNC1 and is essential to prevent autoimmunity in Arabidopsis. *Mol. Plant* *14*, 1733–1744. <https://doi.org/10.1016/j.molp.2021.06.011>.
25. Cui, Y., Fang, X., and Qi, Y. (2016). Transportin1 promotes the association of microRNA with ARGONAUTE1 in Arabidopsis. *Plant Cell* *28*, 2576–2585. <https://doi.org/10.1105/tpc.16.00384>.
26. Branon, T.C., Bosch, J.A., Sanchez, A.D., Udeshi, N.D., Svinkina, T., Carr, S.A., Feldman, J.L., Perrimon, N., and Ting, A.Y. (2018). Efficient proximity labeling in living cells and organisms with TurboID. *Nat. Biotechnol.* *36*, 880–887. <https://doi.org/10.1038/nbt.4201>.
27. Lüdke, D., Roth, C., Kamrad, S.A., Messerschmidt, J., Hartken, D., Appel, J., Hörnich, B.F., Yan, Q., Kusch, S., Klenke, M., et al. (2021). Functional requirement of the Arabidopsis importin-alpha nuclear transport receptor family in autoimmunity mediated by the NLR protein SNC1. *Plant J.* *105*, 994–1009. <https://doi.org/10.1111/tpj.15082>.
28. Contreras, R., Kallemi, P., González-García, M.P., Lazarova, A., Sánchez-Serrano, J.J., Sanmartín, M., and Rojo, E. (2019). Identification of domains and factors involved in MINIYO nuclear import. *Front. Plant Sci.* *10*, 1044. <https://doi.org/10.3389/fpls.2019.01044>.
29. Koncz, C., Dejong, F., Villacorta, N., Szakonyi, D., and Koncz, Z. (2012). The spliceosome-activating complex: molecular mechanisms underlying the function of a pleiotropic regulator. *Front. Plant Sci.* *3*, 9. <https://doi.org/10.3389/fpls.2012.00009>.
30. Chanarat, S., and Sträßer, K. (2013). Splicing and beyond: the many faces of the Prp19 complex. *Biochim. Biophys. Acta* *1833*, 2126–2134. <https://doi.org/10.1016/j.bbamcr.2013.05.023>.
31. Lee, J.H., Terzaghi, W., Gusmaroli, G., Charron, J.B., Yoon, H.J., Chen, H., He, Y.J., Xiong, Y., and Deng, X.W. (2008). Characterization of Arabidopsis and rice DWD proteins and their roles as substrate receptors for CUL4-RING E3 ubiquitin ligases. *Plant Cell* *20*, 152–167. <https://doi.org/10.1105/tpc.107.055418>.
32. Fang, Y., and Spector, D.L. (2007). Identification of nuclear dicing bodies containing proteins for microRNA biogenesis in living Arabidopsis plants. *Curr. Biol.* *17*, 818–823. <https://doi.org/10.1016/j.cub.2007.04.005>.
33. Huang, S., Zhu, S., Kumar, P., and MacMicking, J.D. (2021). A phase-separated nuclear GBPL circuit controls immunity in plants. *Nature* *594*, 424–429. <https://doi.org/10.1038/s41586-021-03572-6>.
34. Collier, S., Pendle, A., Boudonck, K., van Rij, T., Dolan, L., and Shaw, P. (2006). A distant coilin homologue is required for the formation of cajal bodies in Arabidopsis. *Mol. Biol. Cell* *17*, 2942–2951. <https://doi.org/10.1091/mbc.e05-12-1157>.
35. Grote, M., Wolf, E., Will, C.L., Lemm, I., Agafonov, D.E., Schomburg, A., Fischle, W., Urlaub, H., and Lührmann, R. (2010). Molecular architecture of the human Prp19/CDC5L complex. *Mol. Cell. Biol.* *30*, 2105–2119. <https://doi.org/10.1128/MCB.01505-09>.
36. de Moura, T.R., Mozaffari-Jovin, S., Szabó, C.Z.K., Schmitzová, J., Dybkov, O., Cretu, C., Kachala, M., Svergun, D., Urlaub, H., Lührmann, R., and Pena, V. (2018). Prp19/Pso4 is an autoinhibited ubiquitin ligase activated by stepwise assembly of three splicing factors. *Mol. Cell* *69*, 979–992.e6. <https://doi.org/10.1016/j.molcel.2018.02.022>.
37. Ohi, M.D., Vander Kooi, C.W., Rosenberg, J.A., Chazin, W.J., and Gould, K.L. (2003). Structural insights into the U-box, a domain associated with multi-ubiquitination. *Nat. Struct. Biol.* *10*, 250–255. <https://doi.org/10.1038/nsb906>.
38. Dressano, K., Weckwerth, P.R., Poretzky, E., Takahashi, Y., Villarreal, C., Shen, Z., Schroeder, J.I., Briggs, S.P., and Huffaker, A. (2020). Dynamic regulation of Pep-induced immunity through post-translational control of defence transcript splicing. *Nat. Plants* *6*, 1008–1019. <https://doi.org/10.1038/s41477-020-0724-1>.
39. Smirnova, E., Marquis, V., Poirier, L., Aubert, Y., Zumsteg, J., Ménard, R., Miesch, L., and Heitz, T. (2017). Jasmonic acid oxidase 2 hydroxylates jasmonic acid and represses basal defense and resistance responses against Botrytis cinerea infection. *Mol. Plant* *10*, 1159–1173. <https://doi.org/10.1016/j.molp.2017.07.010>.
40. Yoshizawa, T., Ali, R., Jiou, J., Fung, H.Y.J., Burke, K.A., Kim, S.J., Lin, Y., Peeples, W.B., Saltzberg, D., Soniat, M., et al. (2018). Nuclear import receptor inhibits phase separation of FUS through binding to multiple sites. *Cell* *173*, 693–705.e22. <https://doi.org/10.1016/j.cell.2018.03.003>.
41. Guo, L., Kim, H.J., Wang, H.J., Monaghan, J., Freyermuth, F., Sung, J.C., O'Donovan, K., Fare, C.M., Diaz, Z., Singh, N., et al. (2018). Nuclear-import receptors reverse aberrant phase transitions of RNA-binding proteins with prion-like domains. *Cell* *173*, 677–692.e20. <https://doi.org/10.1016/j.cell.2018.03.002>.
42. Hofweber, M., Hutten, S., Bourgeois, B., Spreitzer, E., Niedner-Boblentz, A., Schifferer, M., Ruepp, M.D., Simons, M., Niessing, D., Madl, T., and Dormann, D. (2018). Phase separation of FUS is suppressed by its nuclear import receptor and arginine methylation. *Cell* *173*, 706–719.e13. <https://doi.org/10.1016/j.cell.2018.03.004>.
43. Qamar, S., Wang, G., Randle, S.J., Ruggeri, F.S., Varela, J.A., Lin, J.Q., Phillips, E.C., Miyashita, A., Williams, D., Ströhl, F., et al. (2018). FUS phase separation is modulated by a molecular chaperone and methylation of arginine cation- π interactions. *Cell* *173*, 720–734.e15. <https://doi.org/10.1016/j.cell.2018.03.056>.
44. Zavaliev, R., Mohan, R., Chen, T., and Dong, X. (2020). Formation of NPR1 condensates promotes cell survival during the plant immune response. *Cell* *182*, 1093–1108.e18. <https://doi.org/10.1016/j.cell.2020.07.016>.
45. Jung, J.H., Barbosa, A.D., Hutin, S., Kumita, J.R., Gao, M., Derwort, D., Silva, C.S., Lai, X., Pierre, E., Geng, F., et al. (2020). A prion-like domain in ELF3 functions as a thermosensor in Arabidopsis. *Nature* *585*, 256–260. <https://doi.org/10.1038/s41586-020-2644-7>.
46. Tang, Y., Ho, M.I., Kang, B.H., and Gu, Y. (2022). GBPL3 localizes to the nuclear pore complex and functionally connects the nuclear basket with the nucleoskeleton in plants. *PLOS Biol.* *20*, e3001831. <https://doi.org/10.1371/journal.pbio.3001831>.
47. Huang, X., Chen, S., Li, W., Tang, L., Zhang, Y., Yang, N., Zou, Y., Zhai, X., Xiao, N., Liu, W., et al. (2021). ROS regulated reversible protein phase separation synchronizes plant flowering. *Nat. Chem. Biol.* *17*, 549–557. <https://doi.org/10.1038/s41589-021-00739-0>.
48. Yoo, S.D., Cho, Y.H., and Sheen, J. (2007). Arabidopsis mesophyll protoplasts: a versatile cell system for transient gene expression analysis. *Nat. Protoc.* *2*, 1565–1572. <https://doi.org/10.1038/nprot.2007.199>.
49. Huang, A., Tang, Y., Shi, X., Jia, M., Zhu, J., Yan, X., Chen, H., and Gu, Y. (2020). Proximity labeling proteomics reveals critical regulators for inner

- nuclear membrane protein degradation in plants. *Nat. Commun.* *11*, 3284. <https://doi.org/10.1038/s41467-020-16744-1>.
50. Zhang, X., Smits, A.H., van Tilburg, G.B., Ovaas, H., Huber, W., and Vermeulen, M. (2018). Proteome-wide identification of ubiquitin interactions using UbiA-MS. *Nat. Protoc.* *13*, 530–550. <https://doi.org/10.1038/nprot.2017.147>.
51. Kim, D., Paggi, J.M., Park, C., Bennett, C., and Salzberg, S.L. (2019). Graph-based genome alignment and genotyping with HISAT2 and HISAT-genotype. *Nat. Biotechnol.* *37*, 907–915. <https://doi.org/10.1038/s41587-019-0201-4>.
52. Li, H., Handsaker, B., Wysoker, A., Fennell, T., Ruan, J., Homer, N., Marth, G., Abecasis, G., and Durbin, R.; 1000 Genome Project Data Processing Subgroup (2009). The Sequence Alignment/Map format and SAMtools. *Bioinformatics* *25*, 2078–2079. <https://doi.org/10.1093/bioinformatics/btp352>.
53. Love, M.I., Huber, W., and Anders, S. (2014). Moderated estimation of fold change and dispersion for RNA-seq data with DESeq2. *Genome Biol.* *15*, 550. <https://doi.org/10.1186/s13059-014-0550-8>.
54. Wu, T., Hu, E., Xu, S., Chen, M., Guo, P., Dai, Z., Feng, T., Zhou, L., Tang, W., Zhan, L., et al. (2021). clusterProfiler 4.0: A universal enrichment tool for interpreting omics data. *Innovation (Camb)* *2*, 100141. <https://doi.org/10.1016/j.xinn.2021.100141>.
55. Shen, S., Park, J.W., Lu, Z.X., Lin, L., Henry, M.D., Wu, Y.N., Zhou, Q., and Xing, Y. (2014). rMATS: robust and flexible detection of differential alternative splicing from replicate RNA-Seq data. *Proc. Natl. Acad. Sci. USA* *111*, E5593–E5601. <https://doi.org/10.1073/pnas.1419161111>.
56. Dobin, A., Davis, C.A., Schlesinger, F., Drenkow, J., Zaleski, C., Jha, S., Batut, P., Chaisson, M., and Gingeras, T.R. (2013). STAR: ultrafast universal RNA-seq aligner. *Bioinformatics* *29*, 15–21. <https://doi.org/10.1093/bioinformatics/bts635>.

STAR★METHODS

KEY RESOURCES TABLE

REAGENT or RESOURCE	SOURCE	IDENTIFIER
Antibodies		
Anti-HA	Roche	Cat#11867423001; RRID:AB_390918
Anti-GFP	Takara Bio	Cat#632381; RRID:AB_2313808
Streptavidin (HRP)	Abcam	Cat#ab7403
Goat anti-mouse IgG-HRP secondary antibody	Thermo Scientific	Cat#31430; RRID:AB_228307
Goat anti-rat IgG-HRP secondary antibody	Thermo Scientific	Cat#31470; RRID:AB_228356
Bacterial and virus strains		
<i>Agrobacterium tumefaciens</i> GV3101	Sheng Luan Lab	N/A
<i>Pseudomonas syringae</i> pv. <i>tomato</i> DC3000	Ksenia Krasileva lab	N/A
<i>Pseudomonas syringae</i> pv. <i>tomato</i> DC3000 <i>AvrRpt2</i>	Ksenia Krasileva lab	N/A
<i>Pseudomonas syringae</i> pv. <i>tomato</i> DC3000 <i>AvrRps4</i>	Jennifer Lewis lab	N/A
Chemicals, peptides, and recombinant proteins		
TRIzol Reagent	Invitrogen	Cat#15596018
cComplete Mini, EDTA-free	Roche	Cat#11836170001
MG132	Sigma	Cat#M7449
Dynabeads™ Myone™ streptavidin C1	Invitrogen	Cat#65002
Murashige&Skoog Basal Medium (MS)	Caisson Labs	Cat#MSP09
Dexamethasone	Sigma	Cat#D4902
Biotin	Sigma	Cat#B4501-1G
Macerozyme R-10	Yakult pharmaceutical IND. CO	Macerozyme™ R-10
Cellulase R-10	Yakult pharmaceutical IND. CO	Cellulase Onozuka™ R-10
Zeocin	Thermo Scientific	Cat#J67140-XF
Critical commercial assays		
PrimeSTAR GXL DNA Polymerase	Takara Bio	Cat#R050B
ClonExpressII One Step Cloning Kit	Vazyme	Cat#C112
Maxima First Strand cDNA Synthesis Kit	Thermo fisher	Cat#K1672
PowerUp SYBR Green Master Mix	Thermo fisher	Cat#A25742
QuikChange II Site-Directed Mutagenesis Kit	Agilent	Cat#200523
NucleoBond Xtra Midi EF	Takara Bio	Cat#740420
Direct-zol RNA Miniprep Kit	Genesee Scientific	Cat#11-330
Deposited data		
Raw data for RNA-Seq (WT, <i>ka120</i>)	Jia et al. ²⁴	GEO: GSE147683
Raw data for proximity labeling proteomics (KA120-TurboID)	This paper	ProteomeXchange: PXD040403
Raw data for proximity labeling proteomics (MAC3B-TurboID)	This paper	ProteomeXchange: PXD040403
Raw data for RNA-Seq (WT, <i>p35S:MAC3B^{Q77A/D84A}-GFP #19</i>)	This paper	GEO: GSE224520
Experimental models: Organisms/strains		
<i>Arabidopsis thaliana</i> : WT; Col-0	Xinnian Dong lab	N/A
<i>p35S:KA120-YFP / ka120</i>	Jia et al. ²⁴	N/A
<i>p35S:KA120-mCherry / Col-0</i>	Jia et al. ²⁴	N/A
<i>p35S:SAD2-GFP / Col-0</i>	This paper	N/A
<i>pKA120:KA120-TurboID / ka120</i>	This paper	N/A
<i>pSAD2:SAD2-TurboID / sad2</i>	This paper	N/A
<i>p35S:KA120-BioID / ka120</i>	This paper	N/A
<i>p35S:IMB5-BioID / imb5</i>	This paper	N/A
<i>ka120</i>	Jia et al. ²⁴	Salk_148803

(Continued on next page)

Continued

REAGENT or RESOURCE	SOURCE	IDENTIFIER
<i>cdc5-1</i>	Palma et al. ¹³	Salk_207_F03
<i>pr1-2</i>	Palma et al. ¹³	Salk_039427
<i>mos4-1</i>	Palma et al. ¹³	CS69914
<i>mac3a mac3b</i>	Monaghan et al. ¹²	CS69985
<i>mac8 CRISPR</i>	This paper	N/A
<i>snc1-r1</i>	Yuelin Zhang Lab	N/A
<i>ka120 cdc5-1</i>	This paper	N/A
<i>ka120 pr1-2</i>	This paper	N/A
<i>ka120 mac3a mac3b</i>	This paper	N/A
<i>ka120 mos4</i>	This paper	N/A
<i>ka120 snc1-r1 mac3a mac3b</i>	This paper	N/A
<i>mac3a mac3b snc1-r1</i>	This paper	N/A
<i>ka120 mac8 CRISPR</i>	This paper	N/A
<i>imb5</i>	Jia et al. ²⁴	Salk_206109
<i>sad2</i>	Jia et al. ²⁴	Salk_133577
<i>g6pd6-1</i>	ABRC	Salk_016157
<i>g6pd6-2</i>	ABRC	Salk_024885
<i>irr-1</i>	ABRC	Salk_015201
<i>parp2</i>	ABRC	Salk_140400
<i>zin1</i>	Jennifer Lewis lab	Salk_137325
<i>bhlh3</i>	ABRC	Salk_050954
<i>jao2-1</i>	ABRC	Salk_206337
<i>ka120 g6pd6-1</i>	This paper	N/A
<i>ka120 g6pd6-2</i>	This paper	N/A
<i>ka120 irr-1</i>	This paper	N/A
<i>ka120 parp2</i>	This paper	N/A
<i>ka120 zin1</i>	This paper	N/A
<i>ka120 bhlh3</i>	This paper	N/A
<i>ka120 jao2-1</i>	This paper	N/A
<i>pCDC5: CDC5-GFP / ka120 +/-</i>	This paper	N/A
<i>pPRL1: PRL1-GFP / ka120 +/-</i>	This paper	N/A
<i>pMAC3B: MAC3B-GFP / ka120 +/-</i>	This paper	N/A
<i>pMOS4: MOS4-GFP / ka120 +/-</i>	This paper	N/A
<i>pSKIP: SKIP-GFP / ka120 +/-</i>	This paper	N/A
<i>pMAC8: MAC8-GFP / ka120 +/-</i>	This paper	N/A
<i>pCDC5: CDC5-GFP / p35S: KA120-mCherry</i>	This paper	N/A
<i>pPRL1: PRL1-GFP / p35S: KA120-mCherry</i>	This paper	N/A
<i>pMAC3B: MAC3B-GFP / p35S: KA120-mCherry</i>	This paper	N/A
<i>pMOS4: MOS4-GFP / p35S: KA120-mCherry</i>	This paper	N/A
<i>pSKIP: SKIP-GFP / p35S: KA120-mCherry</i>	This paper	N/A
<i>pMAC8: MAC8-GFP / p35S: KA120-mCherry</i>	This paper	N/A
<i>p35S: MAC3B-GFP / Col-0</i>	This paper	N/A
<i>Dex: amiRNA-KA120 / p35S: MAC3B-GFP</i>	This paper	N/A
<i>pHYL1: HYL1-mCherry / p35S: MAC3B-GFP / Dex: amiRNA-KA120</i>	This paper	N/A
<i>p35S: Coilin-mCherry / p35S: MAC3B-GFP / Dex: amiRNA-KA120</i>	This paper	N/A
<i>p35S: SR45-mRFP / p35S: MAC3B-GFP / Dex: amiRNA-KA120</i>	This paper	N/A
<i>pMAC3B-MAC3B-TurboID / ka120 +/-</i>	This paper	N/A
<i>p35S: MAC3B^{O77A/D81A}-GFP / Col-0</i>	This paper	N/A

(Continued on next page)

Continued

REAGENT or RESOURCE	SOURCE	IDENTIFIER
p35S:MAC3B ^{Q77A/D81A} -GFP / mac3a mac3b	This paper	N/A
p35S:MAC3B ^{H31/D34A} -GFP / Col-0	This paper	N/A
Oligonucleotides		
See Table S7		
Recombinant DNA		
pEarleyGate-pSAD2:SAD2-TurboID	This paper	N/A
pEarleyGate-pKA120:KA120-TurboID	This paper	N/A
pEarleyGate-p35S:IMB5-BioID	This paper	N/A
pEarleyGate-p35S:KA120-BioID	This paper	N/A
pBAV154-amiRNA-KA120	Jia et al. ²⁴	N/A
pEarleyGate100-35S:KA120-YFP	Jia et al. ²⁴	N/A
pCambia1300-p35S:SAD2-GFP	This paper	N/A
pCambia1300-p35S:MAC3B-GFP	This paper	N/A
pCambia1300-p35S:MAC3B ^{Q77A/D81A} -GFP	This paper	N/A
pCambia1300-p35S:MAC3B ^{H31A/D34A} -GFP	This paper	N/A
pCambia1300-pMAC3B:MAC3B-GFP	This paper	N/A
pCambia1300-pCDC5:CDC5-GFP	This paper	N/A
pCambia1300-pPRL1:PRL1-GFP	This paper	N/A
pCambia1300-pMOS4:MOS4-GFP	This paper	N/A
pCambia1300-pSKIP:SKIP-GFP	This paper	N/A
pCambia1300-pMAC8:MAC8-GFP	This paper	N/A
pCambia1300-pMAC3B:MAC3B-TurboID	This paper	N/A
pCambia1300-p35S:KA120-mCherry	Jia et al. ²⁴	N/A
pBI-pHYL1:HYL1-mCherry	This paper	N/A
pBI-p35S:Coilin-mCherry	This paper	N/A
pROK2-ATSR45-mRFP	ABRC	CD3-795044
pUC18-p35S:GFP	This paper	N/A
pUC18-p35S:mCherry	This paper	N/A
pUC18-p35S:gMAC3B-GFP	This paper	N/A
pUC18-p35S:cMAC3B-GFP	This paper	N/A
pUC18-p35S:Ubox-GFP	This paper	N/A
pUC18-p35S:CC-GFP	This paper	N/A
pUC18-p35S:WD40-GFP	This paper	N/A
pUC18-p35S:Ubox-CC-GFP	This paper	N/A
pUC18-p35S:Ubox-CC ^{D34A} -GFP	This paper	N/A
pUC18-p35S:Ubox-CC ^{P39A} -GFP	This paper	N/A
pUC18-p35S:CC-WD40-GFP	This paper	N/A
pUC18-p35S:gMAC3B-CC-GFP	This paper	N/A
pUC18-p35S:-KA120-mCherry	Jia et al. ²⁴	N/A
pGBKT7-KA120	This paper	N/A
pGADT7-MAC3B	This paper	N/A
pGADT7-Ubox	This paper	N/A
pGADT7-CC	This paper	N/A
pGADT7-WD40	This paper	N/A
pGADT7-Ubox-CC	This paper	N/A
pGADT7-Ubox-CC ^{D34A}	This paper	N/A
pGADT7-Ubox-CC ^{P39A}	This paper	N/A
pGADT7-CC-WD40	This paper	N/A
pGADT7-CDC5	This paper	N/A
pGADT7-PRL1	This paper	N/A

(Continued on next page)

Continued

REAGENT or RESOURCE	SOURCE	IDENTIFIER
<i>pGADT7-MOS4</i>	This paper	N/A
<i>pGADT7-MAC5A</i>	This paper	N/A
<i>pGADT7-SKIP</i>	This paper	N/A
<i>pGADT7-MAC8</i>	This paper	N/A
Software and algorithms		
GraphPad 8	GraphPad Software	https://www.graphpad.com/scientific-software/prism/
Image J	NIH	scientific-software/prism/
R v4.0.3	R Core Team	https://www.R-project.org/
trim-galore v0.6.6	GitHub	https://github.com/FelixKrueger/TrimGalore
HISAT2 v2.2.0	HISAT2	http://daehwankimlab.github.io/hisat2/
Samtools v1.9	Samtools	http://www.htslib.org/
rMATS v4.1.1	GitHub	https://github.com/Xinglab/rmats-turbo
DEP v1.12.0	R package DEP	https://bioconductor.org/packages/release/bioc/html/DEP.html
DESeq2 v1.30.1	R package DESeq2	https://bioconductor.org/packages/release/bioc/html/DESeq2.html
clusterProfiler v3.18.1	R package clusterProfiler	https://bioconductor.org/packages/release/bioc/html/clusterProfiler.html
ggplot2 v3.3.5	R package ggplot2	https://ggplot2.tidyverse.org/
Alphafold2	GitHub	https://github.com/deepmind/alphafold

RESOURCE AVAILABILITY

Lead contact

Further information and requests for resources and reagents should be directed to and will be fulfilled by the lead contact, Yangnan Gu (guyangnan@berkeley.edu).

Materials availability

Materials used in this study are available from the [lead contact](#) upon reasonable request. This study did not generate new unique reagents.

Data and code availability

- Raw data files for the RNA-seq have been deposited into the NCBI GEO under accession number GEO: GSE224520 and are publicly available. Raw data files for all mass spectrometry analyses have been deposited to the ProteomeXchange Consortium via the iProX partner repository (ProteomeXchange: PXD040403) and are publicly available.
- This study did not generate code requiring public database deposition.
- All other data that support the findings of this study are available within the article and its [supplemental information](#) and from the [lead contact](#) upon reasonable request.

EXPERIMENTAL MODEL AND STUDY PARTICIPANT DETAILS

Plants

All WT, mutant, and transgenic *Arabidopsis thaliana* plants are in the Col-0 background. Plants were grown either on Sunshine Mix#4 soil or on ½ MS medium (Caisson Labs) with 1% agar and 1% sucrose (pH 5.7) under a light cycle 12h light/12h dark at 22°C. Seeds were surfaced-sterilized with 10% (v/v) bleach for 5 min and washed thoroughly in sterile water 6 times before germinating on MS medium. The *cdc5-1*, *prl1-2*, *mos4-1*, *mac3a mac3b*, *g6pd6-1*, *g6pd6-2*, *irr-1*, *parp2*, *bhlh3*, and *jao2-1* mutants were obtained from Arabidopsis Biological Resource Center (ABRC), and their double or triple mutants with *ka120* were obtained through genetic crosses. The *snc1-r1* and *zin1* mutant was obtained from Yuelin Zhang lab and Jennifer Lewis lab, respectively, and the *ka120 snc1-r1 mac3a mac3b*, *mac3a mac3b snc1-r1*, and *ka120 zin1* mutants were obtained through genetic crosses. The *ka120 mac8* double mutant was obtained by transforming *MAC8* CRISPR construct directly into the *ka120* mutant. All primers for mutant genotyping are listed in [Table S7](#).

Microbe strains

Escherichia coli strain DH5 α was grown at 37°C in Luria Broth medium with antibiotics, the resistance to which is conferred by the plasmid.

Agrobacterium tumefaciens strain GV3101 was grown at 28°C in Luria Broth medium with antibiotics, the resistance to which is conferred by the plasmid.

Pseudomonas syringae pv. *tomato* strain DC3000 was grown at 28°C in a modified Luria Broth medium with antibiotics as described.

Saccharomyces cerevisiae strain Y187 and AH109 were grown at 30°C in yeast extract-peptone-dextrose-adenine medium or synthetic dropout medium as described.

METHOD DETAILS

Plasmid construction

To create the *mac8* mutant, we employed two distinct CRISPR guide RNAs specifically targeting the *MAC8* gene. These were integrated into the forward and reverse primers used for PCR, with the *pCBC-DT1T2* vector serving as the template. Purified PCR products together with the egg cell-specific promoter-driven Cas9 expressing binary vector *pHEE401* were used to set up restriction-ligation reactions, resulting in the construct of *pHEE401-MAC8*.

To generate fluorescence protein-tagged constructs, the promoter sequences and full-length genomic DNA of *CDC5 / PRL1 / MAC3B / MOS4 / SKIP / MAC8* were inserted into a modified binary vector *pCambia1300* with the GFP tag at the C terminus by In-Fusion cloning (ClonExpress II One Step Cloning Kit, Vazyme). Those constructs were transformed into *ka120* heterozygous plants via *Agrobacterium tumefaciens* strain GV3101 and isogenic transgenic lines in WT and *ka120* backgrounds were obtained through segregation in the next generation. Those lines in the WT background were subsequently crossed with the *p35S: KA120-mCherry / Col-0* line. For colocalization with MDNCs, the promoter sequences and full-length genomic DNA of *Coilin* and *HYL1* were inserted into *pBI111L-mCherry*. The *35S:SR45-mRFP* construct was obtained from ABRC. These constructs were transformed into the *p35S:MAC3B-GFP / Dex:amiRNA-KA120* background. In addition, the constitutive 35S promoter-driven *SAD2-GFP* and *MAC3B-GFP* constructs were transformed into WT background.

To generate BioID2 and TurboID constructs, the promoter sequences and full-length genomic DNA of *KA120*, *SAD2*, and *MAC3B* were inserted into a modified binary vector pEarleyGate with the TurboID-HA tag at the C terminus by In-Fusion cloning. The full-length genomic DNA of *KA120* and *IMB5* were inserted into pEarleyGate with the BioID2-HA tag at the C terminus by In-Fusion cloning. These constructs were transformed into corresponding mutant backgrounds. The *pMAC3B-MAC3B-TurboID* construct was transformed into *ka120* heterozygous plants and isogenic transgenic lines in WT and *ka120* backgrounds were obtained through segregation in the next generation to perform the comparative proximity labeling proteomics.

For protoplast transient assays, the full-length genomic DNA of *MAC3B* and the cDNA of *Ubox / CC / WD40 / Ubox-CC / CC-WD40* and their mutant variants were cloned into *pUC18-p35S:GFP* by In-Fusion cloning. To construct the *MAC3B-CC-GFP*, the CC domain was cut from *pUC18-p35S:CC-GFP* with BamHI and inserted into the C-terminal of the full-length *MAC3B* in *pUC18-gMAC3B-GFP*.

For yeast-two-hybrid (Y2H) assays, the full-length cDNA of *KA120* was inserted into *pGBKT7* by restriction enzyme cloning using BamHI and EcoRI. Similarly, the full-length cDNA of *CDC5 / MAC3B / MOS4 / SKIP / MAC8* were cloned into *pGADT7*. The full-length cDNA of *PRL1* and *MAC5A* were inserted into *pGBKT7* by In-Fusion cloning. *MAC3B* truncations were cut from *pUC18-Ubox / CC / WD40 / Ubox-CC / CC-WD40-GFP* and cloned into *pGADT7* with BamHI.

For site-directed mutagenesis, *MAC3B-GFP* in the *pUC18-GFP* vector was mutagenized to *MAC3B^{Q77A/D81A}-GFP* and *MAC3B^{H31A/D34A}-GFP* using the QuikChange II Site-Directed Mutagenesis Kit (Agilent). The mutated *MAC3B* sequence was also cut and cloned into binary vector *pCambia1300-p35S:GFP* with BamHI. These constructs were transformed into WT and *mac3a mac3b* mutant background. Similarly, *U-box* in the *pGADT7* and *U-box-CC* in the *pUC18-GFP* were mutagenized to *U-box^{D34A/P39A}* and *U-box-CC^{D34A/P39A}-GFP*.

All PCR products were obtained using high-fidelity DNA polymerase (PrimeSTAR GXL, Takara Bio). All primers for cloning are listed in Table S7.

Protoplast transfection

Plasmids used for protoplast transfection were purified using NucleoBond Xtra Midi EF (Takara Bio). Arabidopsis mesophyll protoplasts were prepared and transfected as previously described.⁴⁸ Briefly, 3-week-old Arabidopsis leaves were sliced and digested in enzymolysis solution containing 3% cellulase R-10, 0.8% macerozyme R-10 (Yakult pharmaceutical IND. CO), and 0.4M mannitol for 6 hours to produce protoplasts. For co-transfections, 10 μ g of each plasmids were used to transfect 200 μ l protoplasts (2×10^5 / ml). After transfection, protoplasts were incubated for 10–12 hours before examined by Zeiss LSM710 equipped with a 63x oil objective lens.

RNA extraction and RT-qPCR

For RT-qPCR, total RNA was extracted from plant tissues using TRIzol RNA reagent (Invitrogen). First-strand cDNA was synthesized from 1 μ g of total RNA using the Maxima First Strand cDNA Synthesis Kit (Thermo Fisher). qPCR was performed using PowerUp SYBR Green Master Mix (Thermo Fisher). Primers used for qPCR are provided in [Table S7](#). *ACT2* was used as the reference gene.

Pathogen infection

PstDC3000, *PstDC3000/AvrRps4*, and *PstDC3000/AvrRpt2* were grown at 28°C on a modified LB medium containing 25 μ g/mL rifampicin (adding 50 μ g/mL kanamycin if *PstDC3000* carries Avr genes). For pathogen growth measurement, leaves of four-week-old *Arabidopsis* plants were hand-infiltrated with bacterial suspension of $OD_{600nm} = 0.001$. On the day of inoculation (day 0) and 3 days past inoculation (day 3), four leaf discs from four independent plants were pooled as one sample. Four samples and eight samples were collected per genotype per treatment on day 0 and day 3, respectively. The samples were ground in 500 μ l 10 mM $MgCl_2$. Serially diluted samples were plated on a modified LB medium containing the appropriate antibiotics. Bacterial colonies were counted 2 days after growing at 28°C. The colony-forming units (cfu) were normalized by leaf area (per cm^2).

To image pathogen-induced MDNC formation or to test KA120 protein level in response to pathogen infection, leaves of 4-week-old *p35S:MAC3B-GFP* or *pKA120-KA120-YFP* transgenic plants were infiltrated with bacterial suspension of *PstDC3000* ($OD_{600nm} = 0.01$) and *PstDC3000* carrying *AvrRpt2* or *AvrRps4* ($OD_{600nm} = 0.01$). Fluorescence images of MAC3-GFP were taken 2 days after incubation by Zeiss LSM710 equipped with a 63x oil objective lens. Protein level of KA120-YFP were detected with immunoblot using anti-GFP antibody (Takara) and goat anti-mouse IgG-HRP secondary antibody (Thermo Scientific).

Drug treatment

For zeocin treatment, WT and mutant seeds were germinated with or without 2 μ g/ml zeocin (Thermo Scientific) added to 1/2 MS agar plates. For dexamethasone treatment, four-day-old seedlings grown on 1/2 MS agar plates were transplanted into liquid 1/2 MS medium with or without 25 μ M dexamethasone (Sigma). MDNCs were imaged 12 h after incubation.

Yeast two hybrid

Y2H analysis was performed using the Matchmaker GAL4-based Two-Hybrid System 2 (Clontech) according to the manufacturer's instructions. The activation domain fusion (prey) constructs and the DNA-binding domain fusion (bait) constructs were transformed into yeast strains Y187 and AH109, respectively. The yeast cells of Y187 and AH109 containing corresponding constructs were mated in 2 \times YPDA medium at 30°C for 24 h before being plated. Diploid yeasts were grown on double (SD-Leu-Trp) or quadruple (SD-Leu-Trp-Ade-His) dropout media or triple dropout (SD-Leu-Trp-His) media containing 3 mM 3-amino-1, 2, 4-Trizole (3AT) at 30°C for 5 to 7 days.

FRAP analysis

The *p35S:MAC3B-GFP / Dex:amiRNA-KA120* double transgenic seedlings were grown on 1/2 MS medium for 5 days before being transferred into liquid MS medium with 25 μ M dex. FRAP of dex-induced MDNCs in *Arabidopsis* root cells was performed on a Zeiss LSM880 using the 63x objective. MDNCs were bleached using a laser intensity of 100% at 488 nm with 100 iterations. Fluorescence recovery was recorded for 10 min with 5 s intervals after bleaching. Images were acquired using ZEN software. Analyses of the mean fluorescence intensity of the bleached region were carried out using ImageJ and the recovery curve was drawn using GraphPad 8. For time-lapse microscopy of the MDNC fusion, images were recorded every 1 s for 15 min by LSM710 equipped with a 63x oil objective lens.

Proximity labeling proteomics

Seedlings of *p35S:KA120-BioID2-3HA / ka120*, *p35:IMB5-BioID2-3HA / imb5*, *pKA120:KA120-TurboID-3HA / ka120*, and *pSAD2:SAD2-TurboID-3HA / sad2*, transgenic plants were grown on 1/2 MS plates for 10 days. *pMAC3B:MAC3B-TurboID-3HA / Col-0* and *pMAC3B:MAC3B-TurboID-3HA / ka120* transgenic plants were grown on 1/2 MS plates for two weeks. The whole seedlings were transferred into 1/2 MS liquid medium with or without 50 μ M of free biotin (Sigma) for 16 hours for BioID2 or 5 hours for TurboID. About 0.5 g of treated seedlings were harvested as one replicate for each sample, and two biological replicates were collected for each sample. Samples were frozen in liquid nitrogen and stored at -80°C until use. The proximity labeling, protein extraction, and subsequent streptavidin-based affinity purification, on-beads trypsin digestion, and mass spectrometry were performed as described previously.⁴⁶ Briefly, seedlings were treated with 50 μ M free biotin solution for proximity labeling or incubated with water as mock treatment. After that, the extraction of total protein was accomplished using a protein extraction buffer comprising 50 mM Tris (pH 7.5), 150 mM NaCl, 0.5% Triton X-100, 0.5% Nonidet P-40, 0.5% Nadeoxycholate, a plant protease inhibitor cocktail (cOmplete, Roche), 1 mM PMSF, and 40 mM MG132. To eliminate any free biotin, PD-10 desalting columns (Cytiva) were employed. The resultant eluted protein fraction was subsequently mixed with streptavidin-coated magnetic beads (Dynabeads MyOne Streptavidin C1, Invitrogen), with an overnight incubation at 4°C. This was followed by a meticulous washing process involving five repetitions, utilizing the protein extraction buffer. The affinity-purified samples were then boiled with loading buffer containing 50 μ M biotin and 1% SDS for 30 minutes. Subsequent to this, SDS-PAGE separation was performed. A 5% aliquot was used for western blot with anti-HA antibody (Roche) and goat anti-rat IgG-HRP secondary antibody (Thermo Scientific) for detection of the bait protein expression. Another 5% aliquot was used for western blot with streptavidin-HRP (Abcam) to confirm inducible

biotinylation and successful affinity purification. The rest of samples were loaded on a separate gel and the resultant protein gels were stained using Coomassie blue R-250. For each lane, the gel was divided into three sections, which were individually subjected to trypsin digestion within a 50 mM ammonium bicarbonate solution, maintained at 37°C throughout an overnight period. The ensuing peptides were subjected to extraction using 1% formic acid in a 50% aqueous solution of acetonitrile, and the extracts were subsequently dried using a Speedvac before sending to LC-MS/MS analysis. A detailed proteomic analysis procedure was described previously.^{49,50}

RNA-seq

For RNA-Seq, 7-day-old WT and *p35S:MAC3B^{Q77A/D81A}-GFP* seedlings were collected, and total RNA was extracted using the Direct-zol RNA Miniprep kit. Library construction, quality control, and RNA sequencing were performed by Novogene (<https://en.novogene.com/>) on an Illumina HiSeq 2000 platform. The raw RNA-seq reads generated were filtered using trim-galore v0.6.6 with the default parameters to remove low-quality reads. Cleaned data were then mapped to the *Arabidopsis thaliana* genome TAIR10 using HISAT2 v2.2.0⁵¹ with default parameters. BAMs were sorted by Samtools v1.9.⁵²

Protein structure prediction

Protein complexes were modeled using AF2complex (version 1.4.0), which relies on AlphaFold2. Homologous sequences were collected from comprehensive databases, and all experimental protein structures downloaded from the Protein Data Bank, were considered as structural templates.

QUANTIFICATION AND STATISTICAL ANALYSIS

Statistical analysis

Mean ± S.D. was determined for variables exhibiting a normal distribution, including plant sizes, fluorescence intensity, and log-transformed bacterial cfu. The figure legends comprehensively outline the numbers of technical and biological replicates, along with the corresponding context the numbers represent. Statistical analysis using Student's t-tests or one-way ANOVA followed by Tukey's multiple comparison tests were performed using GraphPad 8.

Proximity labeling proteomics analysis

We collected the protein enrichment areas data (label-free quantification – LFQ intensities) and the peptide spectrum match (PSM) data, which were integrated, normalized, and analyzed by R package DEP using mock treatment or other karyopherin samples as the control.⁵⁰ For KA120 proximiome, the thresholds of differentially probed proteins were set as fold change > 4, *p*-adjust < 0.1, and PSM ≥ 2 for TurboID, and fold change > 4, *p*-adjust < 0.05, and PSM ≥ 3 for BioID2. For MAC3B proximiome, the thresholds of differentially probed proteins were set as fold change > 2, *p*-value < 0.1, and PSM > 2.

RNA-seq analysis

DEGs were analyzed using R package DESeq2 v1.30.1⁵³ with cutoffs *p*-value < 0.1 and log₂(fold change) > 1 to select differentially expressed genes. GO enrichment analysis was performed using R package clusterProfiler v3.18.1.⁵⁴ Fold enrichment is the ratio of GeneRatio versus BgRatio (Background Ratio). Volcano plots and bubble plots were generated by R package ggplot2 v3.3.5.

Alternative splicing analysis

The alternative splicing (AS) events were identified using rMATS v4.1.1^{55,56} with the absolute IncLevelDifference value > 0.1 and false discovery rate (FDR) < 0.05 for *ka120* and *ka120 pad4-1* compared to WT and the absolute IncLevelDifference value > 0.1 and *p*-value < 0.05 for *p35S:MAC3B^{Q77A/D81A}-GFP* compared to WT. IncLevelDifference was the difference in mean Inclusion level (IncLevel) between the sample and the control. All the IncLevels were calculated using normalized counts.

Cell Host & Microbe, Volume 31

Supplemental information

**Nuclear transport receptor KA120 regulates
molecular condensation of MAC3 to coordinate
plant immune activation**

Min Jia, Xuanyi Chen, Xuetao Shi, Yiling Fang, and Yangnan Gu

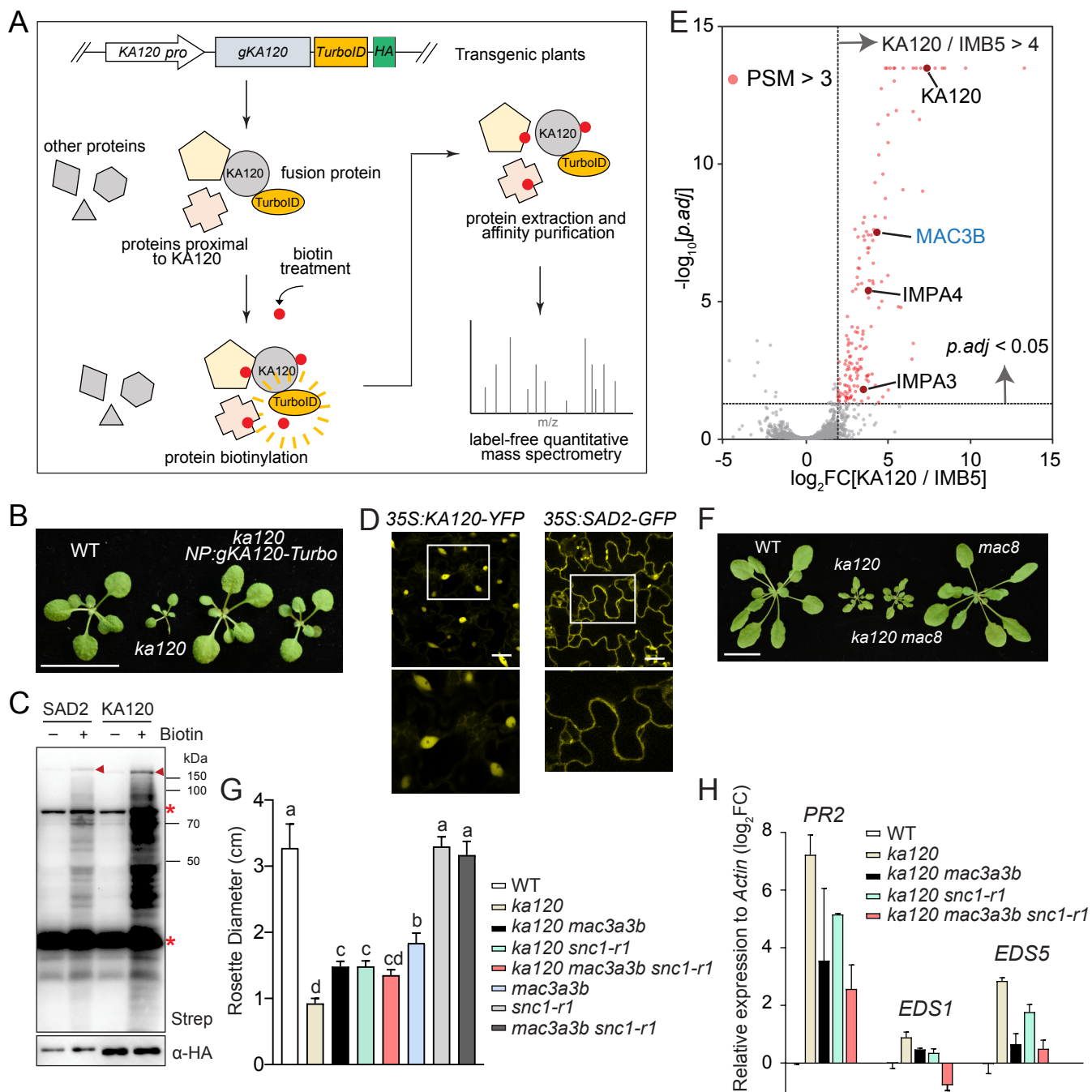


Figure S1. Profiling of KA120 proxime and suppression of *ka120*-dependent autoimmunity by *mac* mutants, Related to Figure 1

(A) Schematic diagram for the identification of KA120 proximal proteins using proximity labeling proteomics.

(B) Complementation of *ka120* mutant phenotypes by the *pKA120-KA120-TurboID-HA* construct in transgenic Arabidopsis plants. Three-week-old plants were shown. Scale bar, 2 cm.

(C) Inducible biotinylation of protein in the *KA120-TurboID* and *SAD2-TurboID* transgenic plants. Transgenic seedlings were treated with 50 μ M free biotin or water for 5 hours before total protein was extracted and subjected to immunoblots with HRP-conjugated streptavidin and anti-HA antibody. Arrowheads indicate self-biotinylated bait protein, and asterisks indicate naturally biotinylated proteins.

(D) Subcellular localization of fluorescence protein-tagged SAD2 and KA120 in transgenic plants. Images from leaf epidermal cells were shown. Enlarged view of white boxes was shown below. Scale bars, 20 μ m.

(E) Volcano plot of significantly enriched protein identified by proximity labeling proteomics using *35S:-KA120-BioID2* transgenic plants. Data from *35S:IMB5-BioID2* transgenic plants were used as control. KA120-specific preys were selected using cutoffs PSM > 3, *p*-value < 0.05, and fold change > 4 compared to IMB5 data and are represented as pink dots.

(F) Four-week-old soil-grown WT, *ka120-1*, *mac8*, and *ka120 mac8* plants. Scale bar, 2 cm.

(G) Measurement of rosette diameter in three-week-old plants. Data are presented as mean \pm SD (*n* = 10). Statistical analysis was performed using one-way ANOVA followed by Tukey's multiple comparisons tests.

(H) The relative expression level of *PR2*, *EDS1*, and *EDS5* in three-week-old plants measured by RT-qPCR. Data are presented as mean \pm SD (*n* = 3 biological replicates)

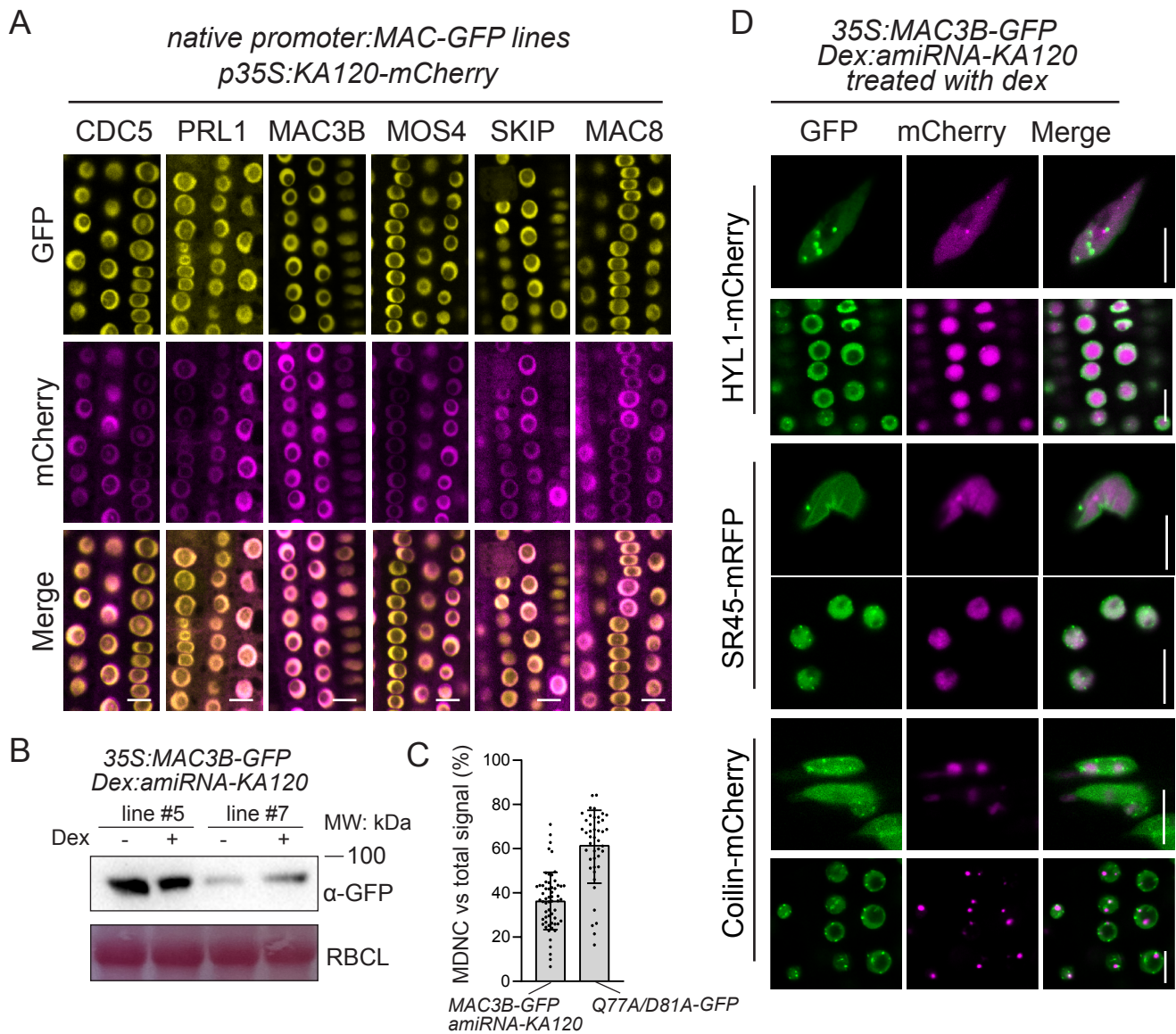


Figure S2. Localization of MAC proteins and the MDNC, Related to Figure 2

(A) Subcellular localization of MAC-GFP proteins in an isogenic *KA120-mCherry* overexpression background. Root cells were imaged in one-week-old seedlings. Scale bars, 10 μ m.

(B) Protein level of MAC3B-GFP measured by immunoblot using *35S:MAC3B-GFP / Dex:amiRNA-KA120* transgenic plants. Plants were treated with water (-) or 25 μ M dex (+) for 12 hours before sampling. Two independent transgenic lines were used.

(C) Fluorescence quantification of MDNCs compared to the total MAC3B signal using cells from *35S:MAC3B-GFP / Dex:amiRNA-KA120* transgenic plants (n = 59) and *35S:MAC3B^{Q77A/D81A}-GFP* transgenic plants (n = 44).

(D) Co-localization of stably expressed nuclear condensate markers (HYL1 for dicing bodies, SR45 for splicing bodies, and Coilin for Cajal bodies) with MAC3B condensates induced in the *35S:MAC3B-GFP / Dex:amiRNA-KA120* double transgenic plants. The transgenic line was treated with 25 μ M dex for 24 hours before images were taken. For each line, root cells in the mature zone and meristem are shown in the upper and lower panel, respectively. Scale bars, 10 μ m.

A



B

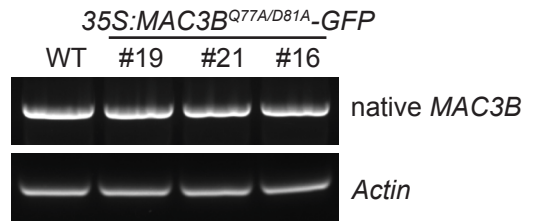


Figure S4. Characterization of *MAC3B*^{Q77A/D81A}-GFP transgenic plants, Related to Figure 4

(A) Phenotype of three independent *35S:MAC3B*^{Q77A/D81A}-GFP transgenic lines in WT background. Four-week-old soil-grown plants are shown. Scale bar, 2 cm.

(B) RT-PCR showing that the expression level of native *MAC3B* in the three *35S:MAC3B*^{Q77A/D81A}-GFP transgenic lines was not silenced by transgene expression compared to WT.

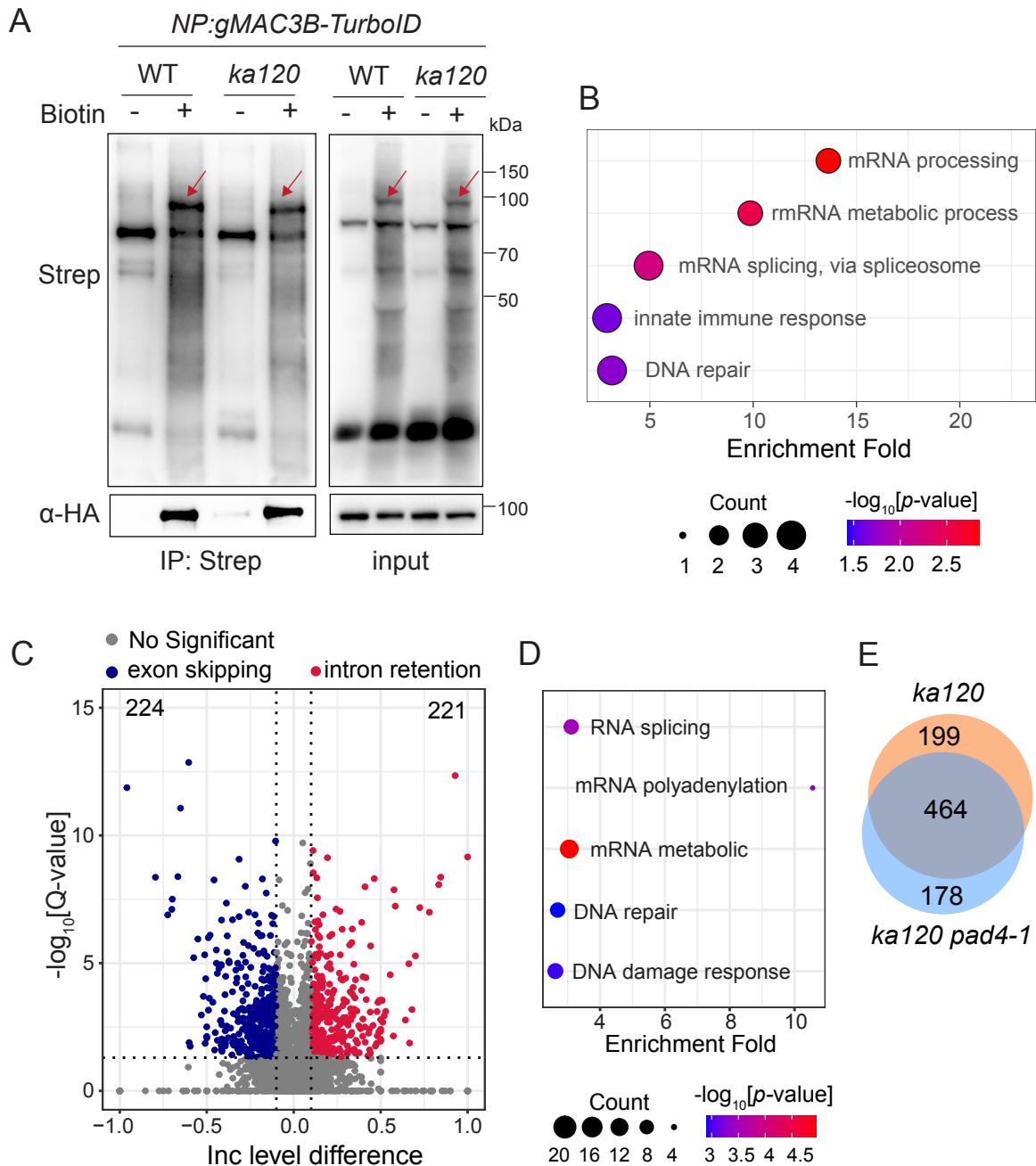


Figure S5. The canonical composition and function of the MAC are compromised in MDNCs, Related to Figure 5

(A) Inducible biotinylation of protein by MAC3B-TurboID-HA in WT and *ka120* transgenic plants. Transgenic seedlings were treated with 50 μ M free biotin or water for 5 hours before total protein was extracted. About 5% sample was aliquoted as input and the remaining was subjected to affinity purification by streptavidin-conjugated beads. Immunoblots were performed using HRP-conjugated streptavidin and anti-HA antibody. Arrows indicate self-biotinylated MAC3B-TurboID-HA protein.

(B) GO analysis of MAC3B-probed candidates that were found in WT but not in *ka120* plants. Representative GO terms are presented.

(C) Intron retention events and exon skipping events identified in *35S:MAC3B^{Q77A/D81A}-GFP* plants in the WT background (p -value < 0.05 and absolute IncLevelDifference > 0.1).

(D) GO analysis of mis-spliced genes in (C). Representative GO terms are presented.

(E) Overlap of mis-spliced genes in the *ka120* single mutant and the *ka120 pad4-1* double mutant.

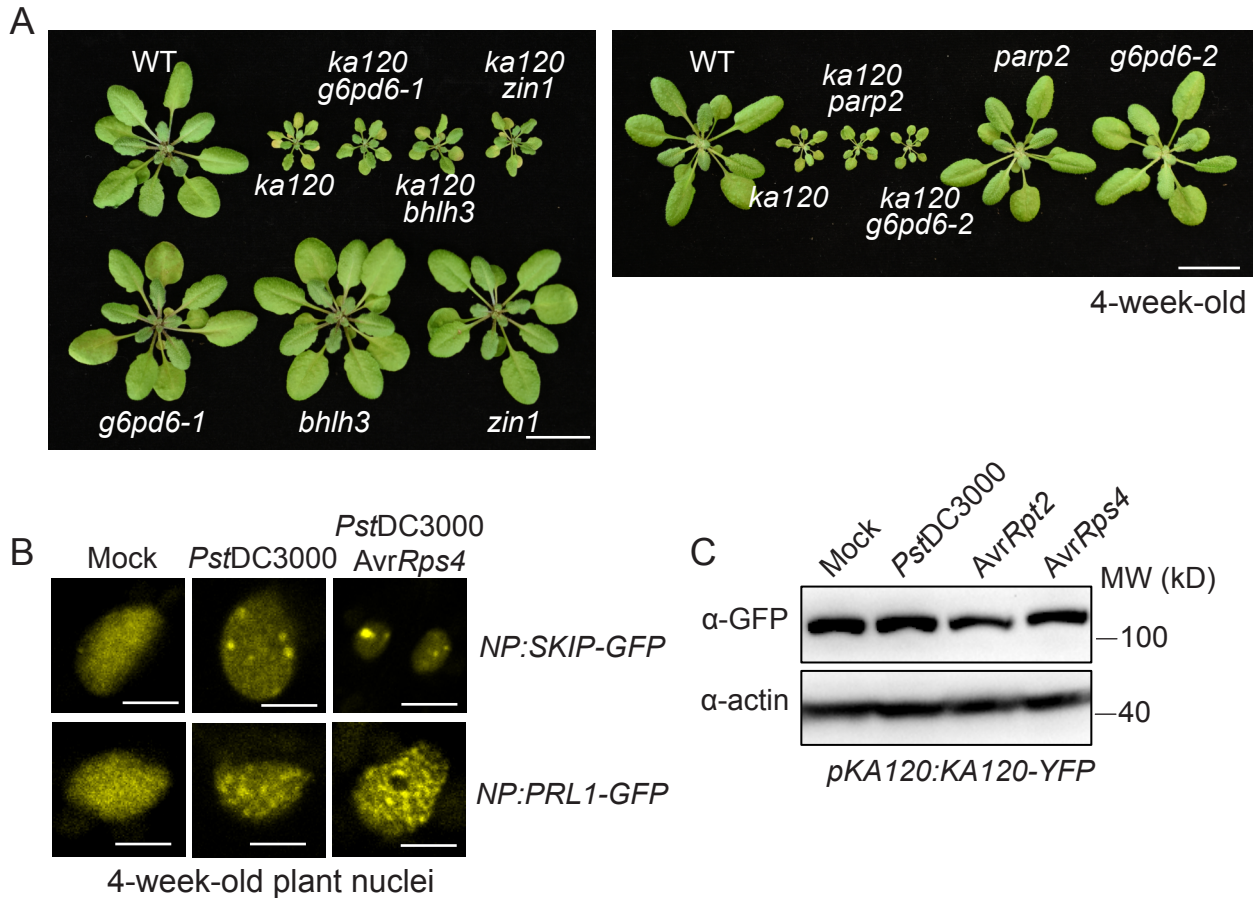


Figure S6. MDNC induction by pathogen-induced immune activation, Related to Figure 6

(A) Four-week-old soil-grown WT and indicated single and double mutant plants. Scale bar, 2 cm.

(B) Induction of MDNCs in native promoter-driven *SKIP-GFP* or *PRL1-GFP* transgenic plants by the bacterial pathogen *PstDC3000* virulent strain ($OD_{600} = 0.01$) and avirulent strain carrying effector *AvrRps4* ($OD_{600} = 0.01$). Nuclei of leaf mesophyll cells of 4-week-old plants are shown. Images were taken 20~24 hours past infection. Scale bars, 5 μ m.

(C) The KA120 protein level before and after pathogen infection. Four-week-old *pKA120-KA120-YFP* transgenic plants were infected by indicated pathogens, and the KA120 protein level was measured by immunoblot using anti-GFP antibody.